Abdullah ORAN PERFORMANCE EVALUATIONS OF SINGLE MODE OPTICAL RECEIVER FOR DEGRADED VISUAL FIELD AND PHOTONIC LANTERN BASED COHERENT DETECTION AGU 2016

PERFORMANCE EVALUATIONS OF SINGLE MODE OPTICAL RECEIVER FOR DEGRADED VISUAL FIELD AND PHOTONIC LANTERN BASED COHERENT DETECTION

A THESIS

SUBMITTED TO THE DEPARTMENT OF ELECTRICAL AND ELECTRONICS ENGINEERING

AND THE GRADUATE SCHOOL OF NATURAL SCIENCES OF ABDULLAH GUL UNIVERSITY

IN PARTIAL FULFILLMENT OF THE REQUIREMENTS

FOR THE DEGREE OF

MASTER

By

Abdullah ORAN

August 2016

PERFORMANCE EVALUATIONS OF SINGLE MODE OPTICAL RECEIVER FOR DEGRADED VISUAL FIELD AND PHOTONIC LANTERN BASED COHERENT DETECTION

A THESIS
SUBMITTED TO THE DEPARTMENT OF ELECTRICAL AND ELECTRONICS ENGINEERING
AND THE GRADUATE SCHOOL OF NATURAL SCIENCES OF ABDULLAH GUL UNIVERSITY
IN PARTIAL FULFILLMENT OF THE REQUIREMENTS
FOR THE DEGREE OF
MASTER

By
Abdullah ORAN
August 2016

SCIENTIFIC ETHICS COMPLIANCE

I hereby declare that all information in this document has been obtained in accordance with academic rules and ethical conduct. I also declare that, as required by these rules and conduct, I have fully cited and referenced all materials and results that are not original to this work.

Abdullah ORAN

REGULATORY COMPLIANCE

M.Sc. thesis titled **"PERFORMANCE EVALUATIONS OF SINGLE MODE OPTICAL RECEIVER FOR DEGRADED VISUAL FIELD AND PHOTONIC LANTERN BASED COHERENT DETECTION"** has been prepared in accordance with the Thesis Writing Guidelines of the Abdullah Gül University, Graduate School of Engineering & Science.

Prepared By — Advisor

Abdullah ORAN — Assoc. Prof. İbrahim Tuna ÖZDÜR

Head of the Electrical and Electronics Engineering Graduate Program

Prof. Bülent YILMAZ

ACCEPTANCE AND APPROVAL

M.Sc. thesis titled **"PERFORMANCE EVALUATIONS OF SINGLE MODE OPTICAL RECEIVER FOR DEGRADED VISUAL FIELD AND PHOTONIC LANTERN BASED COHERENT DETECTION"** and prepared by Abdullah ORAN has been accepted by the jury in the Electrical and Electronics Engineering Graduate Program at Abdullah Gül University, Graduate School of Engineering & Science.

31 / 08 / 2016

JURY:

Assoc. Prof. İbrahim Tuna ÖZDÜR :…….

Prof. Enise AYYILDIZ :…….

Assoc. Prof. Vehbi Çağrı GÜNGÖR :…….

APPROVAL:

The acceptance of this M.Sc. thesis has been approved by the decision of the Abdullah Gül University, Graduate School of Engineering & Science, Executive Board dated ….. /….. / …….. and numbered ……..……. .

….. /….. / ……..
Graduate School Dean

Prof. İrfan ALAN

ABSTRACT

PERFORMANCE EVALUATIONS OF SINGLE MODE OPTICAL RECEIVER FOR DEGRADED VISUAL FIELD AND PHOTONIC LANTERN BASED COHERENT DETECTION

Abdullah ORAN
MSc. in Electrical and Electronics Engineering
Supervisor: Assoc. Prof. İbrahim Tuna ÖZDÜR

August-2016

Imaging at degraded visual environments is one of the biggest challenges in today's imaging technologies. Especially military and commercial rotary wing aviation is suffering from impaired visual field in sandy, dusty, marine and snowy environments. For example, during landing the rotor churns up the particles and creates dense clouds of highly scattering medium, which limits the vision of the pilot and may result in an uncontrolled landing. The vision in such environments is limited because of the high ratio of scattered photons over the ballistic photons that have the image information. In this thesis, we propose to use optical spatial filtering (*OSF*) method in order to eliminate the scattered photons and mainly collect the ballistic photons at the receiver. OSF is widely used in microscopy; to the best of our knowledge this thesis will be the first application of OSF for macroscopic imaging. Our experimental results show that most of the scattered photons are eliminated using the spatial filtering in a highly scattering degraded visual field. The results are compared with a standard broad area photo detector which shows the effectiveness of spatial filtering.

Free space optical systems have applications in different areas such as laser ranging, three-dimensional imaging, weather predictions and optical wireless communication. Some applications require very high performance free space optical systems that are not available today. The need of systems with higher performance and lower size, weight and power (SWaP) is the biggest research motivation of free space optical systems. Between various detection techniques,

coherent optical detection comes forward for applications that require high sensitivity and bandwidth. Coherent detection based LIDAR systems have the potential to provide quantum noise limited performance. However coherent systems suffer from poor free space to fiber collection efficiency due to the single mode detection characteristics and small size of the optical fiber. In order to overcome this problem, photonic lantern is introduced to effectively collect the multimode beam coming from free space and convert it to a number of single mode fibers. The photonic lantern consists of a multimode fiber to a number of single-mode fibers. The collection efficiency enhancement of photonic lanterns have been investigated, however there is no study on the signal to noise ratio –performance- improvement on the photonic lantern based free space coherent systems. In this thesis; the effect of random distribution of the optical power in the 19-port photonic lantern will be investigated mathematically. The photonic lantern based coherent detection system performance will also be simulated by using the MATLAB software. The output of this thesis may open the path to experimental demonstration and maybe even to a prototype.

Keywords: Single mode optical receiver, Degraded visual field, Photonic lantern, LIDAR, Coherent detection.

ÖZET

BOZULMUŞ GÖRSEL ALAN VE FOTONİK FENER TABANLI EŞ FAZLI ALGILAMA İÇİN TEK MODLU OPTİK ALICI PERFORMANS DEĞERLENDİRMESİ

Abdullah ORAN
Elektrik Elektronik Mühendisliği Bölümü Yüksek Lisans
Tez Yöneticisi: Doç. Dr. İbrahim Tuna ÖZDÜR

Ağustos-2016

Bozulmuş görsel ortamlarda görüntüleme günümüz görüntüleme teknolojilerin en büyük zorluklarından biridir. Özellikle döner kanatlı hava araçları kumlu, tozlu, nemli ve karlı ortamlarda iniş esnasında oluşan bozulmuş görsel alanlardan muzdariptirler. Örneğin, iniş sırasında helikopter kanadı yüzünden yerdeki parçacıklar hareket ederek yoğun toz bulutu yani yüksek saçılma ortamı oluşturarak pilotun görüş alanını sınırlar ve kontrolsüz inişe sebep olabilir. Bu tür ortamlarda görüş alanı sınırlı olması, saçılan fotonların görüntü bilgisini taşıyan balistik fotonlara göre yüksek oranda olmasından kaynaklanmaktadır. Bu tezde, saçılan fotonları ortadan kaldırmak ve sadece balistik fotonları toplamak için uzaysal optik filtreleme (*OSF*) metodu önerilmektedir. Bu çalışma, yaygın olarak mikroskoplarda kullanılan OSF metodunun bildiğimiz kadarıyla makroskopik görüntüleme için kullanılmasının ilk araştırması olacaktır. Yapılan deneysel sonuçlarımıza göre bozulmuş görsel alanda saçılan fotonların çoğu kullanılan filtreleme metodu ile elimine edilmiştir. Sonuçlar fotodetektör ile karşılaştırılarak uzaysal filtrelemenin etkinliği gösterilmiştir.

Boş uzay optik sistemleri, lazer ile mesafe ölçme, üç boyutlu görüntüleme, hava durumu tahminleri ve optik kablosuz iletişim gibi uygulamalarından dolayı dikkat çekmektedirler. Yüksek performanslı; daha küçük, daha hafif ve daha az enerji (*SWaP*) tüketen sistemler boş uzay optik sistemlerin en büyük araştırma motivasyonudur. Alıcı teknikleri içerisinde eş-fazlı optik algılama, yüksek

hassasiyet ve hız gerektiren uygulamalarda öne çıkmaktadır. Eş-fazlı algılayıcı tabanlı LIDAR sitemler kuantum gürültü limitli performans sağlayabilmektedir. Buna rağmen, eş-fazlı sistemler tek modlu algılama özelliğinden ve küçük boyutlu optik fiberden dolayı boş uzay ile fiber birleşim verimliliğinin zayıflığından kötü etkilenmektedir. Bu sorunun üstesinden gelmek için, boş uzaydan gelen çok modlu sinyali verimli toplayarak belli sayıda tek modlu fiber dizisine dönüştürebilen fotonik fener kullanılmıştır. Fotonik fenerlerin bir ucu çok modlu fiberden diğer uçları ise birden fazla tek modlu fiberden oluşur Fotonik fener kullanımının optik güç kazancı deneysel olarak ölçülmüş, fakat bu kazanılan optik gücün sistemin sinyal gürültü oranını dolayısıyla da performansını hangi durumlarda nasıl etkileyeceği üzerine bir çalışma yapılmamıştır. Bu tezde; 19 tek modlu fibere sahip fotonik fenerde rastgele olarak dağılmış olan optik gücün sistem performansına nasıl yansıyacağı hesaplanmıştır. MATLAB programı kullanılarak fotonik fener tabanlı eş fazlı algılayıcıların performans simülasyonu yapılmıştır. Bu tez sonucunda elde edilen sonuçlar ve analizler ileride yapılması muhtemel yüksek maliyetli deneysel çalışmalara ışık tutacaktır.

Anahtar kelimeler: Tek modlu optik alıcı, Bozulmuş görsel alan, Fotonik fener, LIDAR, Eş-fazlı Algılama.

Acknowledgements

I'd like to offer my deepest appreciation to my supervisor Assoc. Professor İbrahim T. Özdür for his patience. His guidance helped me in all the time of research and writing of this thesis. And secondly, I thank to Professor Ekmel Özbay for his helpful insight on several occasions. Also, I would also like to acknowledge Researcher Dr. Tolga Kartaloğlu for giving valuable comments on the thesis and the opportunities that we share at Nanotechnology Research Center. I thank my fellow roommates in Abdullah Gül University Ahmet Doğan, Ahmet Özdil, Gökhan Uyan, Hüseyin Emre Erdem, Sinan Genç, Mahmut Büyükbaş, Maruf Göğebakan, Serkan Seven and Yeliz Yoldaş for the interesting discussions and the sleepless mornings we were working together before deadlines, and for all the fun we have had in the last three years. And also I thank my friends: Hüseyin Çilsalar for being always right, Cengiz Gazeloğlu for his problem-solving skills about every aspects of life, Oğuzhan Ayyildiz for our pleasurable conversations about everything from science to relationship. Hatice Taş for her delicious handmade cakes, chocolates and coffee, again Cengiz Gazeloğlu to enlighten us about the magic world of statistics and Mustafa Erkartal to color our office life with his sympathetic behaviors. I also would like acknowledge AGU to give a change doing my thesis. This work is supported by The Scientific and Technological Research Council of Turkey (TUBITAK) Project No: 114E402 and 113C029. Last but not the least; I would like to thank my family: my parents Sefer and Menevşe, for supporting me spiritually throughout my life, and brother and sisters especially Gülşen for their endless supports and love. And finally, as Mark Twain said that "What would men be without women? Scarce, sir...mighty scarce." What would I do without you! I thank you my love, for being in my life.

Table of Contents

List of Figures

List of Tables

Chapter 1

Performance Evaluations of Single Mode Optical Receiver for Degraded Visual Field

One of the biggest challenges in today's imaging technology is three-dimensional (3-D) imaging in degraded visual fields (*DVF*). Especially military and commercial rotary wing aviation is suffering from degraded visual environments in sandy, dusty, marine and snowy environments. In critical mission phases such as take-off and landing accidents are caused by reducing visibilities to near zero due to brownout, whiteout or water spray conditions from obscurant clouds created by the downwash of the rotor blades. Not only in landing but also in flying scenarios heavy fog and snow can easily impair the vision of the pilot. Some examples of degraded visual environments are shown in Figure 1.1.

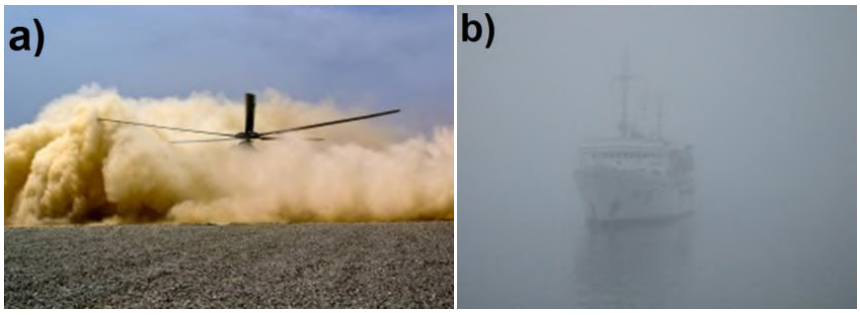

Figure 1.1 Examples of degraded visual environments: rotary wing brown out (Credit: revistaaerea.com) (a), fog in a marine environment (Credit: NOAA) (b).

This vision impairment in rotary wing aviation is resulted in many accidents and life losses in different countries. For example, the UK experienced 24 accidents in the 5 year period of 2005-2009, France has experienced 8 brownout mishaps in the past 15 years, German defense forces has experienced more than 30 mishaps in association with dust or snow. US department of defense report 60 crew members have lost their lives since 1990 due to the visual impairments in degraded visual environments. Many other countries (Canada, Sweden, Norway, and Netherlands) are also report losses and mishap due the degraded visual environments [3].

Degraded visual environments do not only effects rotary wind aviation; people are also affected by fog and snow in daily life especially while driving. According to a report prepared in US, in a 10 year average (2002-2012), 11812 people are injured, 511 people are dead in 31385 crashes ***annually*** in US [4]. One of the notable accidents due to fog was a maritime disaster occurred in 1956, a collision of the ocean liners the SS Andrea Doria and MS Stockholm. As a consequence of the collision 46 people died and SS Andrea Doria capsized and sank [5]. Heavy fog related some other notable accidents are the 1945 crash of a B-25 Mitchell into the Empire State Building [6] and the 1977 collision of Pam Am and KLM planes at the Tenerife Airport [7].

Degraded visual environments are also a problem for subsea investigations. Even for very short distances (a few meters) the visibility can be very poor [8]. These aforementioned cases are main motivations for developing systems to improve the eyesight of pilots, drivers, search and rescue teams, and firefighter.

There are mainly 3 different sensor technologies that offer potential solutions to imaging at degraded visual environments; these technologies are based on RADAR, LIDAR and passive sensors.

RADAR related technologies are based on dust penetration capabilities of mm wave signals (35-95 GHz). Their current limitation is low resolution due to the relatively long wavelength. Because of the strong demand from avionics industry there are commercial products based on this technology, however the research is still going on for better resolution and longer ranges [9]–[11]. The second sensor technology is LIDAR based 3D sensors. These sensors transmit an optical pulse to the area that will be imaged and then detects the reflected optical pulse with fast electronics. When compared with RADAR based sensors, LIDAR based 3D sensor have potential to offer higher resolution and there are promising products from different vendors [12], [13]. The third and the last sensor technology is the passive sensors. Passive sensors rely on thermal imaging but operating at longer wavelengths. Current technologies operate at 94 GHz and exploit naturally reflected and emitted radiation [14].

The LIDAR systems are especially common in 3-D applications such as forest management and planning, flood modeling, determining structural characteristic of land [15] and the Google self-driving car [16]. It can receive an image with high spatial resolution and accuracy remotely; it can detect both ballistic and scattering photons as well. Since; there is no problem of reaching saturation similar with a detector. However; in DVF, the scattering photons may become dominant over the ballistic photons and prevent original image because the LIDAR cannot distinguish the difference between the ballistic and scattering photons. Herein, this thesis presents a method of improving the imaging capabilities in degraded visual environments using a *LIDAR based 3D sensor*. In order to achieve this, we investigated the *optical spatial filtering (OSF)* properties for *coherent* 3D LIDAR architectures.

1.1 LIDAR

To reach the present LIDAR systems, the world of science has spent a lot of years. The scientists entitle the words RADAR (Radiowave-Detection and Ranging), SONAR (Sound-Navigation Ranging) and LIDAR (Light-Detection and Ranging) depending on each emits waves. The only difference among these systems is working in different frequency bandwidths.

Chiroptera, known as bat and many odontocetes can navigate or locate their food, enemies or any objects by echolocation made by animal itself, producing sound waves using their complex genesis systems of nasal sact and passages.

a)

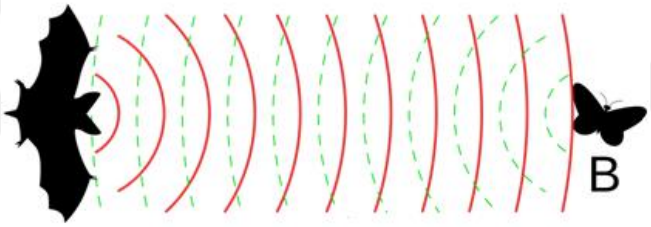

b)

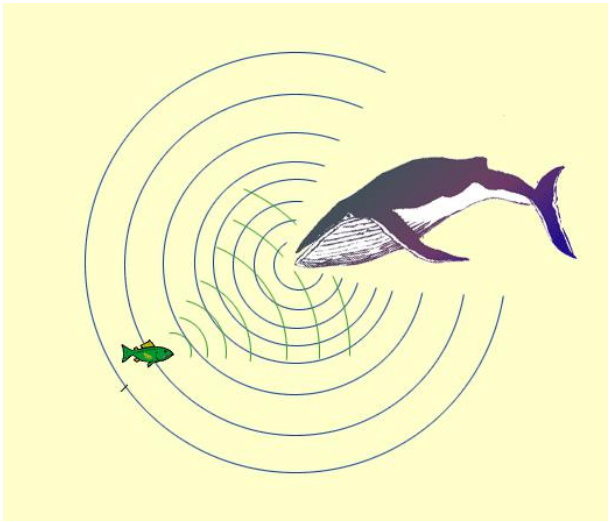

Figure 1.1.1 Bats (a) [1] and odontocetes (b) [2] emit sonar signals in order to locate any object.

Sonar systems are the same idea with echolocation. This system relies on sound waves to locate any objects. Sonar systems are usually used in underwater applications and measure the time delay between the sound emission and the echoes that reflect from the environment [17].

RADAR and LIDAR systems are usually using remote sensing in atmospheric applications compared to Sonar systems. Generally propose of these is calculating position or distance of target. The RADAR system works by transmitting radio waves or microwaves with high pulse power to the object. This pulse is propagated in one direction only with the speed of light by the directivity of antenna. Than it measures how long the bounced signal to return takes. So, the RADAR can determine properties of the object [18].

LIDAR has invented shortly after the laser, originated during the five past decades. “LIDAR” name comes from the first published of LIDAR in the early 1960s which has generated as a portmanteau of "light" and "radar" [19]. LIDAR can combined laser imaging with radar’s ability to observe target or obstacle and calculate the distance by measuring the time of returned signal. LIDAR has been used in meteorology in invested first years for turbulent processes and the diurnal cycle of planetary boundary layer [20]. It also contributes the climatic effects of atmospheric aerosol layer.

LIDAR systems can use not only visible light spectrum region, but also ultraviolet waves (UV: $250nm<\lambda<400nm$) and infrared waves (IR: $700nm<\lambda<1200nm$) from lasers rather than radio waves. Due to the fact that, infrared wavelengths give an advance to provide high resolution and to better penetrate foggy and dusty environments, IR waves are preferred more frequently according to UV waves. LIDAR is popularly used as a high technology (figure 1.1.2). With this feature, the LIDAR systems are using various applications areas which are wind analysis, flood modeling, atmospheric remote sensing, airborne laser scanning, topographical mapping, design autonomous vehicles,

robotics and autonomous navigation, surveying, biology and conservation, mining, search and rescue operations, military, law enforcement and some 3D sensing and imaging systems with high-resolution [21].

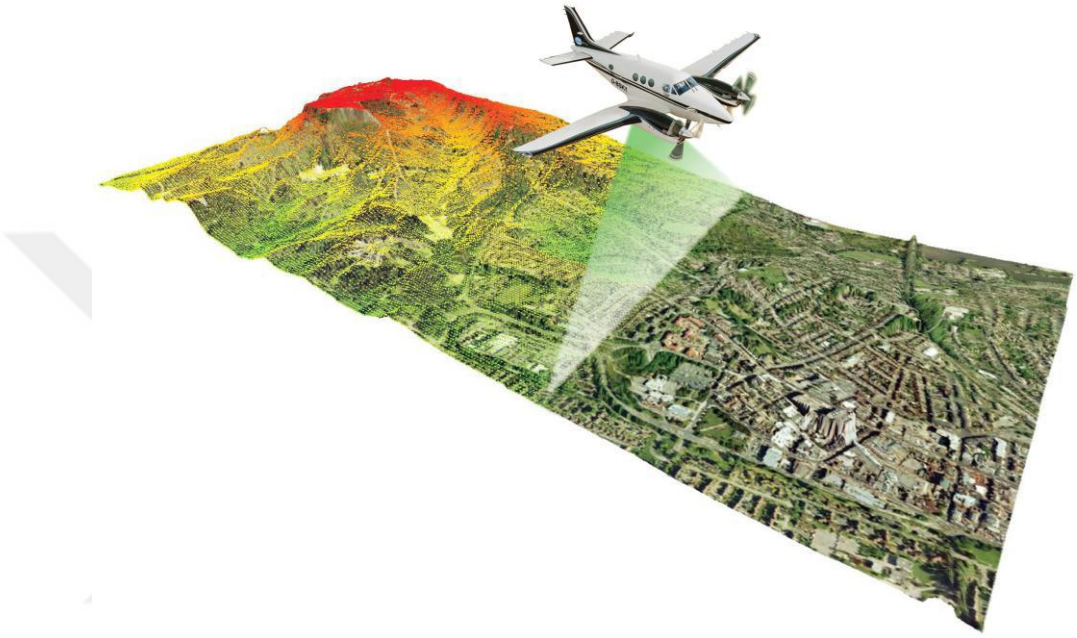

Figure 1.1.2 LIDAR land-scanning system is incorporated on a airplane is using to obtain land surface with high resolution [22].

In another application, a research agency; Agricultural Research Service (ARS) [23]; has been set up for developing a way to colligate LIDAR with agricultural fields. LIDAR technology can be used for improving farmer's yields by creating a topographical map of the agricultural fields which directly shows the slopes and sun exposure of the fields. LIDAR systems also can help farmers to determine which areas need to apply fertilizer. Thus; ARS devoted the farm regions into high, medium or low yield zones according to the quality of agricultural fields.

1.1.1 LIDAR Parameters

Below is a list consists common system parameters of LIDAR sensor that will affect the information gathered. That's why; these parameters are the most challenging parts of a LIDAR system. Get to know these parameters; you can reach a key to success of designing a LIDAR system

Repetition rate: The repetition rate indicates a number that measurement of the pulses per second. Not only laser transmitter puts out the pulses, but also the receiver is sufficiently rapid to get the data from these pulses.

Scanning frequency: the scanner is *oscillating*, or moving forward and backward while the laser is pulsing. The scanning frequency lets you know how fast the scanner is oscillating. Some LIDAR system has a scanner that oscillates continuously in a fixed degree form, but most airborne scanners move forward and backward.

Scanning angle: For some applications, it may be necessary to figure out the scan angle which is measured in degrees and is the distance that the scanner moves from one end to the other. You should modify the angle depending on the application and the accuracy of the desired data item.

Flying attitude: The LIDAR platform is farther from the target. the accuracy of the data will be define the target area. That's the reason for airborne systems, the flying attitude is thereabouts critical.

Flight line spacing: The alternate essential measure is the flight line spacing for airborne systems. The flight line spacing depends on the application.

Nominal point spacing (NPS): It refers to one dimensional measurement i.e. point to point line**.** Point spacing is defined as the distance between two contiguous points. The more points that are taken data in your application, the better the target will be defined. Point density is also impact the point spacing quality. The point spacing varies depending on the application. To the best one's knowledge, LIDAR systems are random sampling systems. Although you cannot adjust exactly which points will be hit on the target field, you can determine how many times the target field will be hit, so you can prefer appropriate frequency of points to better described the targets [24].

We know that there are various types of airborne LIDAR systems. So; in this chapter we have found that the parameters of LIDAR sensor can be manipulated with MATLAB software.

1.1.2 LIDAR Range Equation

Various types for LIDAR receiver systems take advantage about distinctive portions of the signal propagation process. The definition of this process, the LIDAR range equation, is directly similar with the first radar comparison. The LIDAR range equation can be defined with several terms that are effects of various component of the LIDAR architecture.

The LIDAR range equation is generally utilized to compute the received optical power (*Pr*) from target marked by laser pulse containing a transmitter power (*Pt*). The LIDAR range equation has numerous structures that depend on giving a grilled by the LIDAR architecture. The LIDAR equation contains the following aspects of laser propagation, distance, reflection, atmospheric transmission (scattering and absorption), diameter of lens, LIDAR system receiver quantum efficiency and geometry, etc.

An illustration of a LIDAR architecture setup in reference [25] is sketched in figure 1.1.2.1.

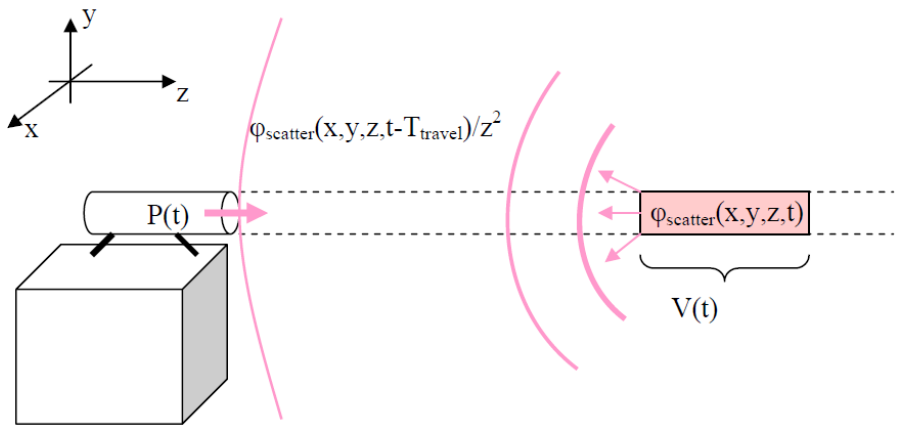

Figure 1.1.2.1 LIDAR architecture setup. P(t) is the transmitted optical power, $\varphi_{scatter}(x,y,z,t)$ is the reflected field scattered.

Also; received optical power by coherent LIDAR system ($\boldsymbol{P_r}$) can be defined as;

$$P_r(t) \approx \eta_{ch} \int_{V(t)} \varphi_{scatter}(x,y,z,t)\, F_{collect}(x,y,z) T(x,y,z)\, dV \quad (1.1.2.1)$$

where η_{ch} describes optical channel loss rate which is detailed in chapter 2.5, $\varphi_{scatter}$ is the scattered optical signal intensity, $F_{collect}$ is the collection efficiency and T is the one way propagation loss which is proportional extinction ratio factor. This equation is described with details in reference [25].

For purpose of this thesis, we will assume the laser transmitter used in typical coherent-detection LIDAR system that has a pulse of laser energy and can exist for a short period. In experimental part, pulse waveform will be considered rectangular in shape and exists for a period of time (typically in nanoseconds, ns) not equal to the pulse width the instantaneous power in watts (W)

transmitted by the LIDAR system *Pt*. All of these are fundamental theoretical tools to describe the optical power output of the LIDAR transmitter.

1.2 Coherent Detection

Free space optical systems attract attention due to their applications which are laser distance measurement [26], 3D imaging [27], weather forecast [20] and optical wireless communication [28]. These working areas have focused on higher performance and lower size, weight and power (SWaP) systems. Some applications, such as laser based face recognition [29], land mine detection and air turbulence effect [30] requires very high performance free space optical systems that are not available today.

Also, military applications such as platforms of satellite systems[31] and lightweight unmanned aerial vehicles (UAVs) [32] have been limited due to the system's size, weight and lack of energy. 3D imaging can be performed in narrow spaces; such as rundown buildings or caves; to search for and provision of aid to people or to do surveillance or intelligence activities by integrating the SWaP systems to the micro and nano UAVs.

A free space optical system has two main parts, transmitter and receiver. Transmitter part is generally simple and similar. Although the transmitter design is relatively straightforward, the system performance is mainly determined by the receiver part. There different receiver method is still used that are direct detection [26], coherent detection [33] and photon counting detection [34].

The most common used detection method is direct detection cause of having cheap materials and easy method of detection. Coherent detection is more preferred in applications that require high precision and speed due to delivering high signal-to-noise ratio. Although photon counting detection is based on high

sensivity detection method; it is much slower according to direct and coherent detection systems. Therefore; the photon counting detection are not preferred for applications requiring high speed such as 3D imaging and optical wireless communication; since very slow.

Coherent detection needs same frequency and phase information with radiation signal. It detects the radiation signal by non-linear mixing with local oscillator. The local oscillator generates a signal with reference frequency and phase. Coherent systems may also consist a time delay, due to some calibrations required in matching reference frequency and phase. This is not the condition with non-coherent systems.

Between various detection techniques, coherent optical detection come forward for applications that requires high sensitivity and wide bandwidth (nearly infrared 700-1600nm). Also; it allows them to actuate at a minimum power. The primary difference between the three types of systems is that in the coherent receiver a portion of the outgoing laser energy is split off and redirected to the receiver detector. Then; this optical source is aligned with the receiver aperture. After that; the coherent detection operates as a classical mixer for two signals; received backscatter and a local oscillator. The output current $i(t)$ of the photodetector can be written as;

$$i(t)_{signal} \propto \eta_{signal}\left(\sqrt{P_{LO}}\cos(\omega_{LO}t) + \sqrt{P_{sig}}\cdot\cos(\omega_{sig}t+\phi)\right)^2 \qquad (1.2.1)$$

where ω_{LO} is the optical frequency of the local oscillator (LO), η_{signal} is a receiver loss and gain factor, ϕ is the relative phase between the signal and LO due to the Doppler effect. Equation is the signal of interest in a coherent system, with the envelope of the signal following the shape of $Ps(t)$ and the signal within the envelope varying at Δv. While the frequency of the optical fields is too high

for any electronic circuits to respond to, modern electronics can easily provide the intermediate frequency in a coherent system.

The force created by all humans putting a foot down at the same harmonious is much stronger than random steps at inharmonious. Likewise, the force of the optical wave or pulse from the coherent beam of LIDAR system is more powerful than that of any single optical wave.

Also shot noise of coherent detection systems is limited. Coherent detection has a local oscillator which helps us to detection signal almost completely overlap. Therefore; a coherent detection system is more complex than other two detection method based LIDAR systems and requires the use of shot noise-limited optics to reach maximum efficiency.

1.3 Research methodology and approach

Imaging through degraded visual environments is a very challenging problem and research and development is still going on. Our approach on the problem is 3D coherent LIDAR technology with optical spatial filtering. Optical spatial filtering is a technique in which a lens focuses an image/beam to a pinhole. In this technique only the beams with the correct wavefront can pass through the pinhole.

Any disturbances on the wavefront will be filtered. One of the main applications of the pinholes is cleaning up laser beams from any unwanted intensity variations [35], Figure 1.3.1a. Another application of optical spatial filtering is to filter out the out-of-focus light. This property is used in confocal microscopy where a laser beam is focused to a focal plane and then a lens and pinhole pair is used to collect light *only from the focal plane* [36], Figure 1.3.1*b*. The wavefront

coming from out-of-focus does not have the correct wavefront for the light to pass through the pin hole.

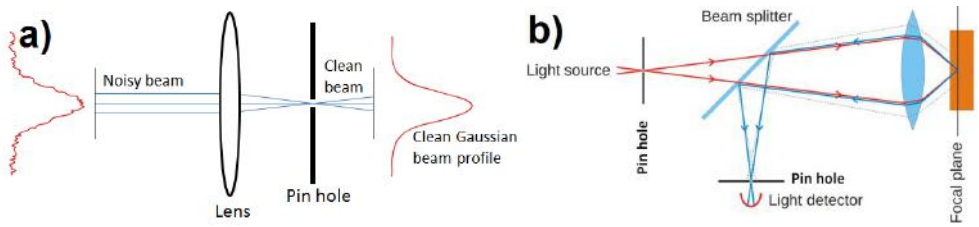

Figure 1.3.1 Application of pin holes: cleaning up Gaussian beams (a) and collecting light only from the focal plane (b).

In this thesis, the intensity noise and out-of-focal light filtering effect was used in order to filter out the scattering light from the receiver.

In a typical 3D imaging LIDAR system, the signal-to-noise ratio is limited by the amount of collected light. In these systems the link loss can be as high as 100 dB, so the amount of receiver optical power is very small and the noise floor is limited by the shot noise or noise of sub-components [37]. In order to increase the amount of collected beam, broad area detectors and multimode fibers are used at the receiver. At degraded visual environments the signal-to-noise ratio (*SNR*) is not limited by the amount of collected light or sub-components but it is limited by the scattered light, that's why increasing the collection efficiency in such systems does not help to solve the problem. In order to eliminate the scattered light we used optical spatial filtering at degraded visual environments.

In the experimental setup, shown in Figure 1.3.2(a and b), an ultra-narrow linewidth (< 1 kHz) laser, working at 1550 nm is used as the light source. An isolator is placed after the laser in order to eliminate any unwanted back reflections. A power splitter is used to measure the power of the laser. The laser beam is sent to the DVF medium using a free space coupler and survived light beams from DVF are measured by different detectors at the back.

a)

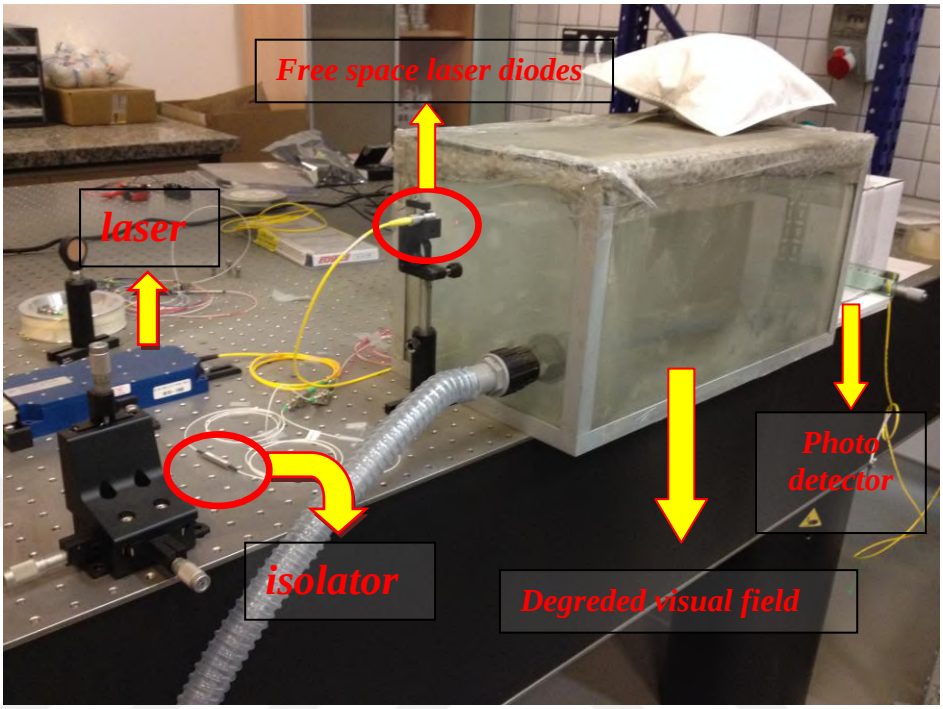

b)

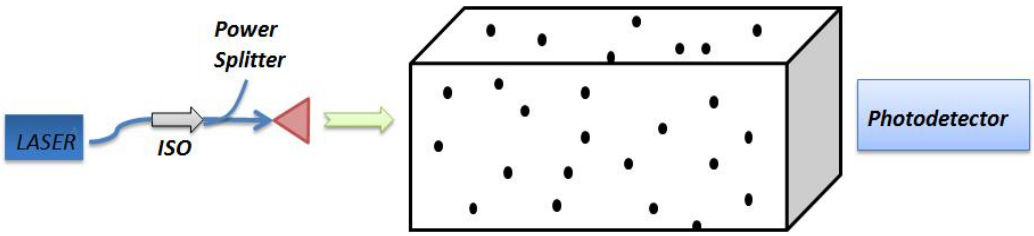

Figure 1.3.2 Experimental setup (ISO: isolator). (a) lab picture (b) illustrated simplify.

The experiments were done in a homemade degraded visual environment. Cement powder is used to create a DVF effect, and particle size distribution of the powder is given in Figure 1.3.3.

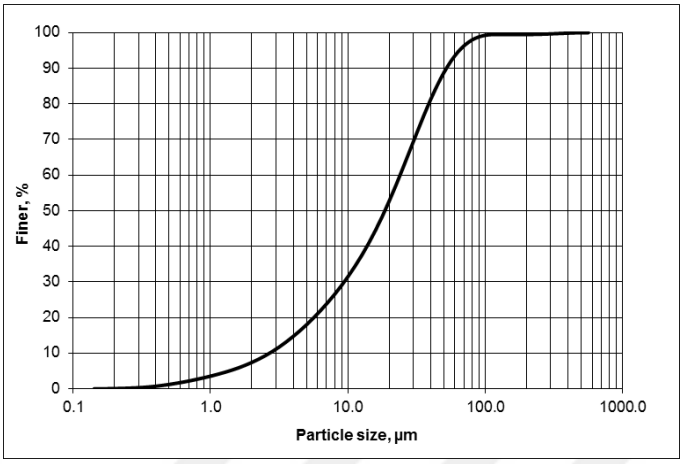

Figure 1.3.3 Particle size of cement used in the experiment.

The experiments were repeated on two separate occasions when the tank is empty and filled with the cement material in order to measure the effectiveness of the optical spatial filtering.

In a degraded visual environment there are two photon types to deal with, the scattering photons and the ballistic photons. The scattering photons reach to the detector after bouncing many times from the particles in the environment. Whereas the ballistic photons arrive directly to the detector without experiencing any scattering. A broad area (or multimode) receiver does not distinguish the scattering and ballistic photons and collect all of them. In Figure 1.3.4, the receiver architecture with a broad area detector is shown. In this setup, all the photons coming from the degraded visual environments, including scattering photon 1 and 2 are detected by the detector which is not desirable for high SNR.

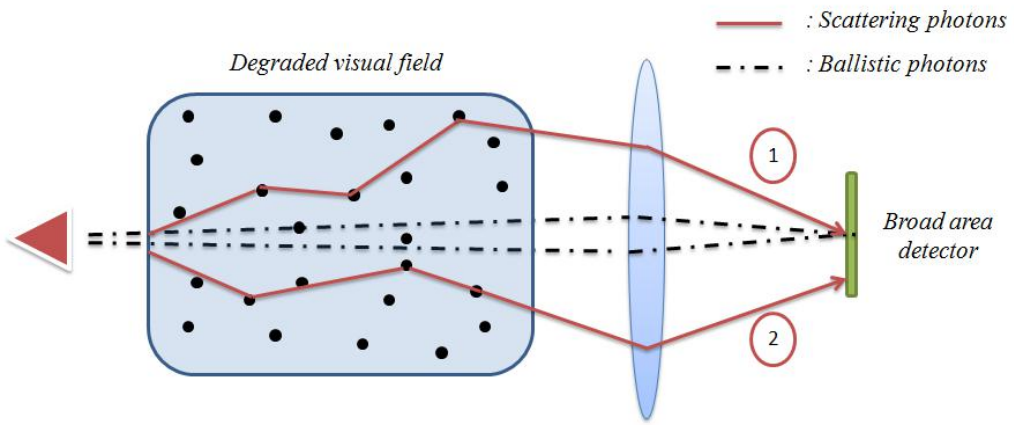

Figure 1.3.4 Receiver architecture with broad area detector (the size is exaggerated) for visual aid.

When the tank is empty and using broad area detector, all the detected photons are ballistic photons and there are no scattering photons. The distribution of the ballistic photons can be seen in figure 1.3.5 black curve; in this figure the x-axis is the distance from the on axis. If the medium is filled with particles then both the ballistic and scattered photons are present at the detection plane. The distribution of the ballistic and scattered photons can be seen in figure 1.3.5 red curve. As expected the collected photons have a broader distribution from the former case which is a result of broad area detection.

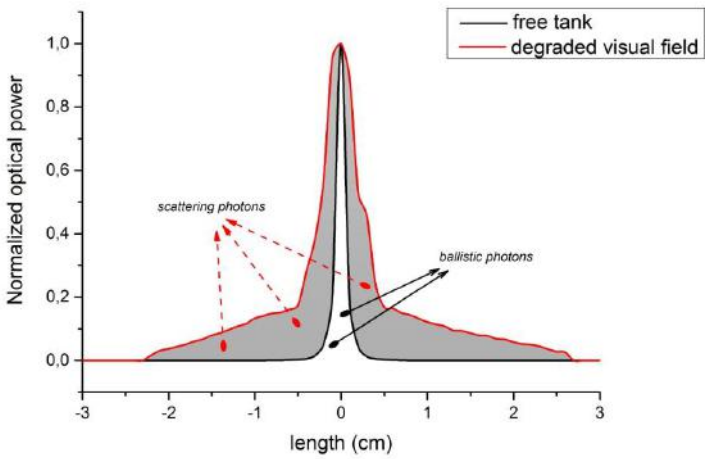

Figure 1.3.5 Optical power of broad area detector for two cases: free tank and DVF.

To eliminate effects of scattering photons, another architecture is prepared. If the transceiver system is focused on the target (shown with blue lines in figure 1.3.6) only the light that is coming from the path of the beam will be coupled back to the fiber, in other words out-of-focus light filtering will be achieved. In coherent LIDAR transceiver architecture less photons are coupled back to the fiber that is why it is not preferable in 3D LIDAR systems. However for 3D imaging at degraded visual environment systems the signal-to-noise ratio of the system is not limited by the amount of light coupled back to the fiber but it is limited by the ratio of scattering photons.

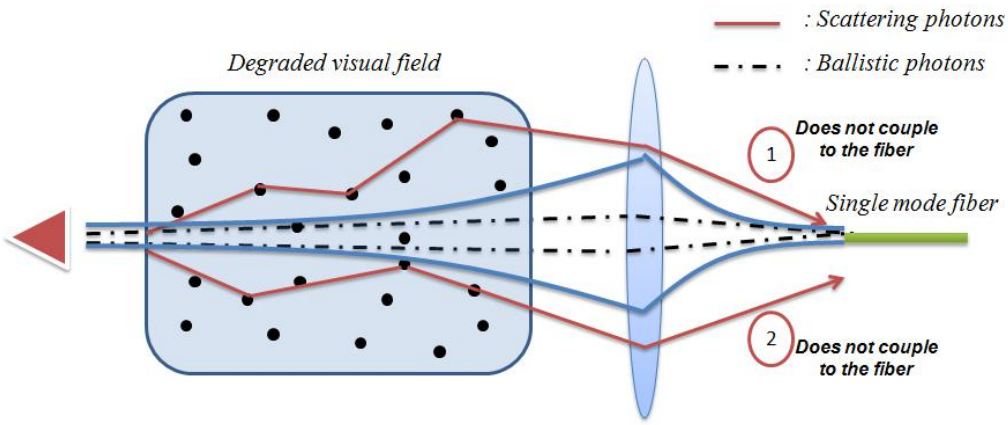

Figure 1.3.6 Receiver architecture with single mode fiber.

In this architecture the scattered light is less likely to couple to the fiber. For example the scattered photon 1 does not couple to the fiber even though it falls on the fiber as it does not have the right $\vec{k}$ vector (or the incoming angle is bigger than the acceptance angle) and photon 2 does not couple to the fiber simply because it does not fall on the fiber. The ballistic beams on the other hand come directly to the fiber and can easily couple to the fiber. In this setup the detected number of ballistic photons are not changing however detected scattered photon number decreases significantly, which will result in a better signal-to-noise ratio. Measured optical power is plotted for different off axis

distances in figure 1.3.7. This figure clearly shows that most of the scattering photons are eliminated by optical spatial filtering method.

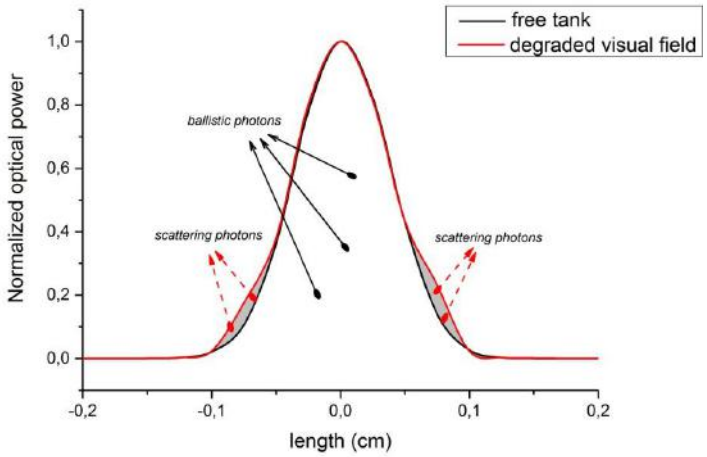

Figure 1.3.7 Optical power of SMF for two cases: free tank and DVF.

1.3.1 System Comparison

Error Results:

The relative error is defined as the ratio of the absolute error, which is defined as the magnitude of the difference between the DVF and the free tank over the magnitude of the ballistic photons. According to values of two Figures (1.3.5 and 1.3.7); error rate are respectively 0.830 and 0.056.

Correlation Results:

All two architecture systems and two cases were simulated and compared based on a projected reach. However, for highest confidence we analyzed two performance comparisons with MATLAB.

Table 1.3.1.1 Significant coefficients of two system performances.

	BAD: free tank	**BAD: DVF**	**SMF: free tank**	**SMF: DVF**
BAD: free tank	1	0.676 0.000	x	x
BAD: DVF	x	1	x	x
SMF: free tank	x	x	1	0.997 0.000
SMF: DVF	x	x	x	1

According to the table 1.3.1.1, there are two hypotheses that can be made comparison for **BAD: free tank** *(data 01)* ~ **BAD: DVF** *(data 02);*

- H_0: There is no significant correlation between the *data 01* and *data 02.*
- H_1: There is a significant correlation between the *data 01* and *data 02.*

The returned value of significant= 0,000<0,05 indicates that H_0 hypothesis is rejected . As a result, there is a significance correlation statistically between *data 01* and *data 02* at the 95% confidence interval as represented in the equation below:

$$r_{data01,data02}=0.676 \qquad (1.3.1.1)$$

For second performance of our system is compared same idea; **SMF: free tank** *(data 03)* ~ **SMF: DVF** *(data 04).*

- H_0: There is no significance correlation between the *data 03* and *data 04.*
- H_1: There is a significance correlation between the *data 03* and *data 04.*

The returned value of significant= 0,000<0,05 indicates that H_0 hypothesis is rejected . As a result, there is a significance correlation statistically between *data 03* and *data 04* at the 95% confidence interval as represented in the equation below:

$$r_{data03,data04}=0.997 \qquad (1.3.1.2)$$

T-Test Results:

Table 1.3.1.2 Distributions of two comparisons.

	Mean	**Variance**
BAD: free tank	39700.5701	7.292e-10
BAD: DVF	5.3533	124.335
SMF: free tank	273938.7574	2.694e-11
SMF: DVF	292.5565	280416.89

Hypothesis test result is returned as a logical value. H=ttest2(x,y) performs a t-test of the hypothesis that two independent samples, in the vectors *BAD: DVF* and *SMF: DVF* (from table 1.3.1.2) represented as x and y , come from distributions with equal means, and returns the result of the test in h.

- If h = 1, this indicates the rejection of the null hypothesis (means $\mu_1= \mu_2$) at the 5% significance level.
- If h = 0, this indicates a failure to reject the null hypothesis at the 5% significance level.

Test the null hypothesis that the pairwise difference between data vectors of **BAD: in case of DVF** and **SMF: in case of DVF** has a mean equal to zero;

```
[h,p] = ttest2(x,y)
>>h =1
>>p =   1.9197e-07                                    (1.3.1.3)
```

The returned value h=1 indicates that *ttest* rejects the null hypothesis at the default 5% significance level. That means, there is significance different statistically between the BAD: in case of DVF and SMF: in case of DVF at the 95% confidence interval.

1.4 Remarks

In this work, we used optical spatial filtering method in order to eliminate scattering photons for degraded visual fields. We compared two different detection schemes, one of them is a broad area detector and the other one is a single mode fiber which has optical spatial filtering effect. Our results show that using the optical spatial filtering effect the ratio of scattering photons are decreased to 5 % from 83 %. The filtering of scattering photons in a scattering medium will improve the imaging performance significantly.

According to this result, we have reached an idea that using SMF in LIDAR imaging system is better than using broad area detector means multi-mode fiber. However; space-to-SMF collection efficiency is not adequate. In chapter 2, we have demonstrated a design with photonic lantern using MATLAB software to improve the space-to-SMF collection efficiency and decrease the bit-error-rate performance of LIDAR architecture.

Chapter 2

Numerical Analysis of Photonic Lantern Based Coherent Detection

Free space optical systems have applications in different areas such as laser ranging, three dimensional (*3D*) imaging, weather predictions and optical wireless communication. Research on this topic is focused on higher performance and lower size, weight and power (SWaP) systems. Some operations, such as land mine detection and laser based face recognition require very high performance free space optical systems that are not available today. Also, current SWaP properties of free space optical systems limit the usage in micro-nano unmanned aerial vehicles and space platforms. The need of systems with higher performance and lower SWaP is the biggest research motivation of free space optical systems. Low SWaP systems can be embedded in surveillance and reconnaissance applications, micro-nano unmanned aerial systems for intelligence, such as 3D imaging in limited space environments. Systems with low SWaP are also ideal for space applications such 3D mapping and high speed optical communication.

Free space optical systems have two main parts: transmitter and receiver. Although the transmitter design is relatively straightforward, the system performance is mainly determined by the receiver. Between various detection techniques, coherent optical detection comes forward for applications that require high sensitivity and bandwidth. Coherent detection systems get the high sensitivity usage of a capable local oscillator at the LIDAR receiver part. In

order to get the highest mixing efficiency in coherent detection systems they need to be mode matched that are the capable local oscillator and the received signal in spatial domain. Free space coherent systems suffer from target or channel-induced speckle, collection efficiency, and multi-mode effects that degrade LO mode matching and reduce system performance [38]. There is nearly no penalty for the use of a single mode fiber (*SMF*) at the collection optics in place of free space detection, substantially because the LO is also a single-mode and the mixing efficiency in SMF is almost 100%. A drawback of SMFs is the poor free space- to-fiber collection efficiency due to the single-mode design of the fiber and small fiber core size, which limits the received optical power [38].

Due to the random fluctuations in the atmosphere and the speckle effect, the optical power distribution through the 19 × SMFs are not equal and constant. Because of the random distribution, the 8 dB higher optical power does not directly map to signal to noise ratio. The collection efficiency enhancement of photonic lanterns has been investigated however there is no study on the signal to noise ratio performance-improvement on the photonic lantern based free space coherent systems. In this thesis, effects of random distributions of the optical power in the 19 × SMFs will be investigated. Two extreme cases (equal optical power distributions in the 19 × SMFs and accumulation of the all optical power in one single fiber) and the random distribution between these two extremes will be analyzed. The photonic lantern based coherent detection system performance will also be simulated by using the MATLAB software. This will be the first simulation on photonic lantern based coherent system [39] simulation in the world. The optical power distribution in the 19 × SMFs will be obtained from the journal that is published in Optics Letters.

The performance improvements of the photonic lantern based photonic systems can effects a great influence the weight, size and power metrics. In this thesis; SWaP improvements of the free space coherent systems will also be

investigated. Also; the performance and SWaP improvements of the photonic lantern based coherent optical systems will be analyzed without using an expensive experimental setup.

The output of this thesis may open the path to experimental demonstration and may be even to a prototype. Development of higher performance and lower SWaP free space coherent systems will make our country stronger in international area.

2.1 Photonic Lantern

In order to use many imaging and optical system technologies effectively, a signal transferring method was needed from single mode to multi mode fibers and vice versa. Multi mode fibers (*MMFs*) are used to collect incoming light from focal plate or atmosphere. It can propagate multiple wavelengths but; SMFs are demanded to separate single wavelengths to supply into a spectrometer. However, an optical device which is fiber Bragg gratings used in SMFs has been observed [40] very poor performance when applied to MMFs. So far, a photonic lantern has been produced [41]–[43] that is able to split MMFs into a large number of SMFs to get high-resolution spectrum. Thus, we can do any single-mode action in MMFs.

The concept of the photonic lantern is similar with multiplexer devices [44]–[46] for space division multiplexing (*SDM*) to provide a smooth transition from a multi-mode core in a single MMF to N single-mode cores in N × SMFs. Optimum performance is achieved when the signals in each N single-mode cores should combine with MMF perpendicularly. The modes are fully mixed and can be resolved with the use of signal processing techniques. Mismatch in mode field diameter between modes in the two waveguides lead to increased

mode depend loss and/or insertion loss during interfacing. Three mode MMF have been demonstrated [47] for SDM that exhibits a 1.5dB improvement.
A study [48] was performed on 3, 12, 15, and 51 core lanterns to couple to 6, 24, 30, and 102 spatial and polarization modes respectively for SDM systems to interface multiple SMFs to a MMF.

The first studies related photonic lantern have been observed during the search for a solution to a problem in astrophysics. Waveform of the optical signal from the outside atmosphere gives valuable information about the content of the gas cloud components, stars and space. This waveform of the optical signal has overwhelmed by narrow emission lines from OH radical that induced radiation of the OH molecule in Earth's upper atmosphere. The best method at present for achieving filter out the OH lines is using a narrow bandwidth optical filter is based on single mode Fiber Bragg Grating (FBG) technology [49]. However, this single mode filtering process to be performed in high performance device such as coherent LIDAR receiver cannot be done very efficiently due to using multi-mode fiber to ensure maximum efficiency in assembling the optical signal from outside atmosphere. Those optical signal fields require a SMF that propagation vectors are aligned with the fiber axis.

To eliminate this problem, photonic lantern has been proposed to use in high performance device that converts light from the multi-mode fiber into a parallel array of SMFs with identical FBGs [50]. As shown in figure 2.1.1, a photonic lantern feeds light to many identical FBGs that constitute the OH-emission filter.

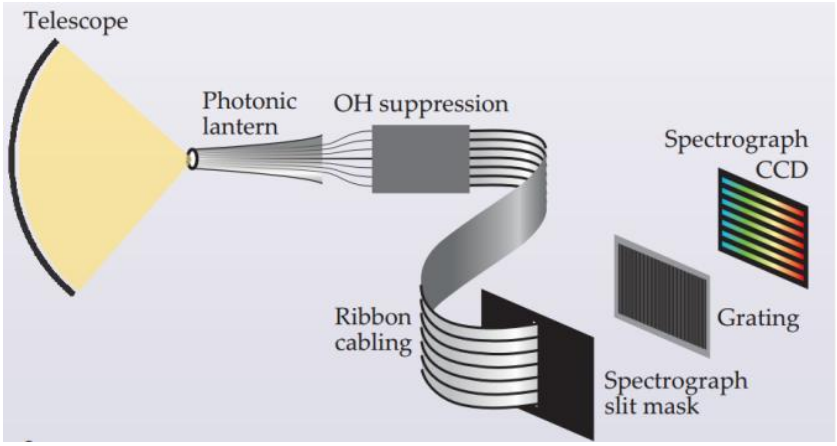

Figure 2.1.1 Use of photonic lantern in telescope: converts multi-mode fiber into an parallel array of SMFs for the OH-emission filter [51].

The photonic lantern is a device that produced by adiabatic tapering a cluster of N several relatively small SMFs. It allows low-loss optical waveguide through its feature that collects light in a large core MMF and convert to N several SMFs [43].

An exemplification of the photonic lantern is shown in Fig. 2.1.2. The photonic lantern is formed three identical parts which are the SMFs, the taper part (or transition region) and the MMF part with the large diameter.

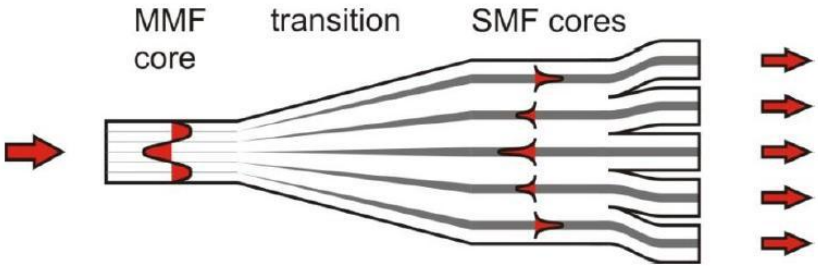

Figure 2.1.2 A schematic diagram of a photonic lantern made by tapering a bundle of SMFs [52].

Optical signal passing through the photonic lantern will follow the transition. The transformation between the different waveguide systems is formed over a

long transition region. This feature gives an advance us to have a uniform light distribution with the tapered end and a low-loss transmission in the device if photonic lantern parameters are reasonably defined [53].

Although photonic lantern is originally developed for astronomical applications [41] to increase the system input aperture while providing single-mode efficiency by collecting the multi-mode end and distributing it into high-resolution N × SMF's such as fiber bragg gratings [54]. These kinds of applications require low coupling losses with very high mode counts. The photonic lantern can be used as both multiplexing and demultiplexing in mode division multiplexed (MDM) systems. Also; the photonic lantern allows us to use end of it's as an input because it is reciprocal. A study was analyzed on two 61-ports photonic lanterns spliced back-to-back provides efficient conversion from a MM fiber into a 61 × SMFs ensemble and back into a MM fiber [42]. This coupling provides a total transmission loss of 0.76 dB at a wavelength of 1530 nm.

Free space coherent optical systems, coherent or intensity modulation/direct detection (IM/DD) systems, suffer from a considerable performance impairment caused by collection efficiency, channel induced speckle, multimode effects and scintillation [39]. Because of the photonic lantern mode transforming properties, it allows to have an improvement of performance on coherent LIDAR systems.

In this thesis we study and analyze the behavior of 19-port photonic lantern which is well-known and the same as the one used in reference [38]. Each SMFs core diameter is determined 5μm. Performance of lantern-based coherent receiver is compared with individual single-mode coherent receivers under the same conditions. Each SMFs of the photonic lantern is connected local oscillator. After using combiner, result of 19 × SMFs is averaged.

2.2 Noises

2.2.1 TIA Noise

In recent years; transimpedance amplifier (TIA) design for high speed data rates has been implemented in numerous works. For instance, the gain bandwidth limit of wideband amplifier has been presented reference [55] and a TIA is attempted in a 0.18- m BiCMOS technology for 10 Gb/s data rate. In addition, an applied design method to be absorbed into passive networks the parasitic capacitances of cascaded gain stages is suggested in reference [55]. The results of reference [55] show that 3-dB bandwidth of 9.2 GHz in the presence of a 0.5 pF photodiode capacitance corresponds to input sensitivity of the TIA is -18 dBm for a bit error rate of 10^{-12} . The bandwidth enhancement ratio is increased 2.4 times.

A 40 Gb/s TIA was executed in 0.18 μm CMOS technology in reference [56]. Measurement of S-parameter observes a transimpedance gain of 51 dBΩ and 3-dB bandwidth up to 30.5 GHz. A bandwidth enhancement technique p-type inductive series peaking (PIP) was presented in reference [56] to improve a bandwidth ratio by a factor of 3.31. Additionally, the noise current response shows that the PIP topology decreases the noise current indirect proportional the frequency increases [56].

The major contributions of the thesis research is a photonic lantern based coherent LIDAR receiver architecture is proposed based on N_{19} SMF x B_e Gb/s parallel communication. TIA noise is considered as the same idea with given references [57], the TIA noise have a transimpedance gain equal to *Ge* (corresponding to absolute temperature and photo detector load resistor) and a noise figure is represented by *NFe*. Electrical filter of bandwidth is represented

with *Be*. The noise is assumed to be a zero-mean Gaussian process. Variance equation the TIA noise equal to;

$$\sigma_{TIA}^2 = \langle i_{TIA}(t) \rangle^2 = (4k_B T/R_L) N F_e B_e \qquad (2.2.1.1)$$

where k_B is the Boltzmann constant, R_L is the photo detector load resistor and T is the absolute temperature. The gain of transimpedance is 500 W, and approximately 3 dB is assumed for TIA noise figure based on measurements of noise statistics and the temperature is calculated to be 333K maximum temperature limit for workplace.

In this thesis; the TIA noise is analyzed and simulated by various bandwidth limited optical signal. Simulation results show that performance of LIDAR systems has been improved, especially in terms of TIA noise. The received optical signal is turned into a photocurrent by photodiode. After the output signal of the photodiode is amplified by a TIA. The primary challenge noise of the light optical signal is the TIA noise that it is critical part of our LIDAR architecture.

2.2.2 Shot Noise

Shot noise is a particular type of noise which degrades fine details of detected optical photons and limits the contrast resolution by making it difficult to detect the small target or obstacle [58].

The variance for TIA photocurrent is calculated in equation 2.2.1.1, while the variance associated with LO shot noise can be expressed as;

$$\sigma_{sh}^2 = 2qR_{pd}P_{LO}B_e \qquad (2.2.2.1)$$

where q is the electronic charge.

The TIA and shot noise is represented as Gaussian process. Therefore;

$$\sigma_{n1}^2 = \langle i_{n1}(t) \rangle^2 = \sigma_{sh}^2 + \sigma_{TIA}^2 \quad (2.2.2.2)$$

The squared current, *I*, again results in an exponential distribution with a mean equal to the total average power

$$\lambda_{no=}\sigma_{n1}^2 \quad (2.2.2.3)$$

Both signal-only and signal+noise PDFs for coherent-detection can be expressed as Gamma distributions. According to our photonic lantern based LIDAR system consists of random Gaussian noise in each N × SMFs being set to 0 to 1. Probability distribution for the N × SMFs sum of independent random quantities is the convolution of the distributions of those quantities. This is applied to determine the exact distribution of the total (and hence the sample mean) of a random sample of *N* Gaussian distributed random quantities.

The exact PDF can be compared to a normal distribution with the same mean and variance, as the sample size *n* increases, thereby illustrating the central limit theorem.

2.3 System Noise Analysis

This chapter presents the noise analysis of our LIDAR system with both SMF and photonic lantern based coherent receiver architectures. We will also refer the description of bit error rate (BER) created by this noise. To the extent that;

the BER estimation is correspondingly degraded if the parameters of LIDAR system are imperfectly estimated.

The noise can be defined as an undesirable disturbance of any optical or electrical signal. The noise sources that can affect an optical communication system are many (e.g. shot noise, speckle noise, TIA noise, thermal noise etc ...) and it is important to know how much the signal is affected by noise. A major parameter that describes the relation between the signal and the noise is the BER. BER is defined as the bit error numbers; which have been altered from any kind of noise, interference, distortion or bit synchronization errors; per all received bits.

The data sequence can be coded according to voltage levels V_L for low level, V_H for high level respectively. If the low level voltage is detected, the information should be 'zero', conversely high level voltage is detected; the information should be 'one'. A noise can chance the voltage levels V_L and V_H. Herein; a bit error occurs in condition when the detection of V_H instead of V_L or vice versa. So; the number of these bit errors creates the bit error rate (BER). It can be also considered as a definition of the probability which a bit value is detected wrong.
Eye diagram is a very useful way of clearly and intuitively understanding the BER analysis [59]. Different bits in a data stream can be represented an eye diagram graph. Consider the figure 2.3.1 below, there are different noises on the channels so that transmitted bit is misidentified at the receiver but, changing in noise probability density functions affects the bit error rates. This situation can be explained as if the more variation occurs in voltage level, the more bit error rate occurs. That means; causes bit errors when it is significant enough to close the pattern eye.

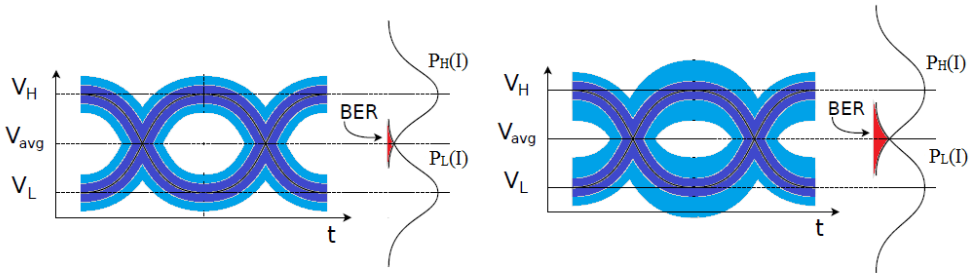

Figure 2.3.1 Eye diagram with different noise (a) small amplitude noise causes small BER (b) large amplitude noise causes large BER.

2.3.1 Mathematical description of the bit error rate

Bit error rate refers to wrong detection or degradation, which may occur over the transmitted signal in optical receiver systems. Bit error rate occurs when the signal level is decreased to a value of the average level by amplitude of the noise or the noise level is raised up to a value of the average level by amplitude of the signal.

$P_L(I)$ and $P_H(I)$ are the probability distribution functions due to the noise fluctuations of respectively the low voltage and the high voltage levels. These two distributions are centered at average signal levels V_H and V_L.
Bit error rate is calculated using following equation;

$$BER = p(signal) \times P(noise \mid signal) + p(noise) \times P(signal \mid noise) \quad (2.3.1.1)$$

where p(x) of transmitting an x (signal or noise) and P(x | y) is the probability of detecting x given that y is sent. The point of decision is taken as the signal wise $V=V_{avg}$. $P_L(I)$ and $P_H(I)$ are respectively the chance that a zero to one occurs ($P_L(I) + P_H(I) = 1$).

To calculate the bit error rate in continuous and discrete probability density functions, we can use following equation;

$$P(signal|noise) = \int_{V_{avg}}^{\infty} p_H(I)dI \sim P[signal|noise] = \sum_{-\infty}^{V_{avg}} p_H[I]$$
$$P(noise|signal) = \int_{-\infty}^{V_{avg}} p_L(I)dI \sim P[noise|signal] = \sum_{-\infty}^{V_{avg}} p_L[I] \qquad (2.3.1.2)$$

Bit error rate will be minimized when threshold is set at intersection of the two probability distribution functions when $d(BER)/dI_{min} = 0$, and is given by;

$$P_L(I_{min})=P_H(I_{min}) = 0.5 \qquad (2.3.1.3)$$

Signal and noise probability distribution functions may occur various fits of distribution. Also, probability of noise and signal may be modifiable system by system. So; it should be able to find the optimal decision threshold level that minimized the BER form. Changeable threshold level gives an advance to develop higher performance and lower SWaP free space coherent LIDAR systems. We present in this thesis that all points of signal and noise distributions can be calibrated as a threshold level to estimate bit error rate (BER) performance of LIDAR systems.

2.4 Data Fitting & Central Limit Theorem

2.4.1 Curve Fitting

This chapter provides information on the method of curve fitting in EasyFit simulation program. It's also known as regression analysis. Curve fitting is used in data analysis and simulation applications including mathematical equations

and nonparametric methods allow fitting sample data stream to common probability distributions. Most of the times, the curve fitting tools produces an equation or parameters that can be used to find points along the curve. Easyfit or Matlab curve fitting toolboxes provide curve fits that can be used in both of these cases. EasyFit simulation program have been choosen our analysis because it lets you analysis your sample data to improve the quality of your fits, and perform with more fitting techniques than Matlab software. So; EasyFit is used for to try and describe both SMF and photonic lantern based LIDAR system complicated data set in fitting data to probability distributions. The tools of EasyFit simulation program provide us with easy ways to calculate probability distributions.

EasyFit can select the best curve fit definition from library of over 50 continuous and discrete distributions, and apply the analysis results to make better decisions, especially if your sample data contains many data points. After the fitting process is accomplished, EasyFit displays the results in the interactive tables and graphs form. The results contain three parts;

- Graphs: displays the output,
- Goodness of fit: the interactive goodness of fit results table,
- Summary: Distribution names and parameter values is defined by fitting results.

The goodness of fit tests evaluates any random data stream whether it is appropriate for a theoretical probability distribution function or not. In other words, GOF tests present for user how well the distribution you select fits to your data.

The results are presented in the form of interactive tables that help you decide which model or type describes your data in the best way. EasyFit calculates the goodness of fit statistics for each of the more than 50 fitted distributions. Then,

program ranks the fitted distributions and displays them in the form of interactive tables.

2.4.2 Demonstration of the Central Limit Theorem

This chapter focus on the main idea of **central limit theorem**[60]. The theorem contains summation of independent and identically-distributed (*IID*) random variables. The Central limit theorem shows how the probability distribution of the summation approaches the normal distribution as the number of terms in the summation increases. Therefore, if the random quantity *X* follows an exponential distribution, with probability density function;

$$f(x;\lambda) = \lambda e^{-\lambda x}\ , (x \geq 0, \lambda > 0)\ \Rightarrow\ E[X] = \frac{1}{\lambda}, V[X] = \frac{1}{\lambda^2} \qquad (2.4.2.1)$$

then the sum *T* of *n* IID random quantities follows the gamma distribution, with probability distribution function (*PDF*).

$$f(t;\lambda,n) = \frac{\lambda\,(\lambda t)^{n-1}e^{-\lambda t}}{(n-1)!},\ (t \geq 0, \lambda > 0, n \in N)$$
$$\Rightarrow\ E[X] = \frac{n}{\lambda}, V[X] = \frac{n}{\lambda^2} \qquad (2.4.2.2)$$

These *n* values of *X* form a random sample of size *n*.

$f_{\bar{X}}(x) = nf_T(nx)$, the PDF of the sample mean $\overline{X}$ is the related function

$$f_{\bar{X}}(t;\lambda,n) = \frac{\lambda n\,(\lambda nx)^{n-1}e^{-\lambda nx}}{(n-1)!},\ (t \geq 0, \lambda > 0, n \in N)$$
$$\Rightarrow\ E[\bar{X}] = \frac{1}{\lambda}, V[\bar{X}] = \frac{1}{n\lambda^2} \qquad (2.4.2.3)$$

For illustration in figure 2.4.2.1, setting λ = 1, the PDF for the sample mean for sample sizes *n* = 1, 2, 4 and 8 are:

$$
\begin{aligned}
n = 1: &\quad f_{\bar{X}}(x) = e^{-x} \\
n = 2: &\quad f_{\bar{X}}(x) = 4xe^{-2x} \\
n = 4: &\quad f_{\bar{X}}(x;\lambda) = \frac{4(4x)^3 e^{-4x}}{3!} \\
n = 8: &\quad f_{\bar{X}}(x;\lambda) = \frac{8(8x)^7 e^{-8x}}{7!}
\end{aligned}
\qquad (2.4.2.4)
$$

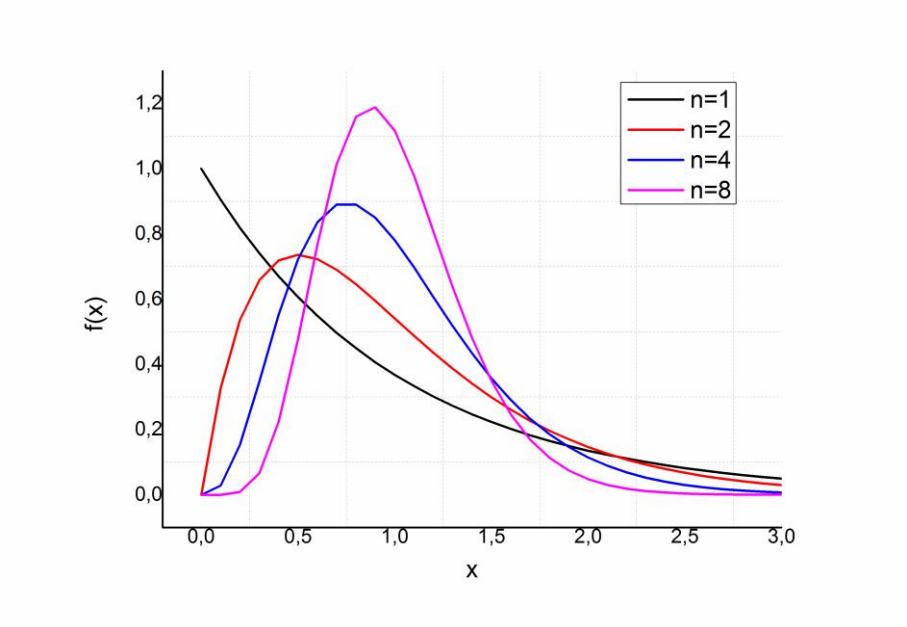

Figure 2.4.2.1 Probability density functions of the sum of n independent exponential random variables for n = 1, 2, 4 and 8.

Note how the inclination of the exponential distribution slowly turns into the normal distribution.

The variance and the positive skew both diminish with increasing sample size. The mean of distributions draw close $\mu = \mathrm{E}[X] = 1$ from the left with increasing sample size for a sample size of $n = 16$, the sample mean $\overline{X}$ has the PDF.

$$f_{\bar{X}}(x) = \frac{16(16x)^{15} e^{-16x}}{15!} \tag{2.4.2.5}$$

and parameters;

$$\mu = \mathrm{E}\left[\bar{X}\right] = 1 \quad \text{and} \quad \sigma^2 = \mathrm{V}\left[\bar{X}\right] = \frac{1}{16} \tag{2.4.2.6}$$

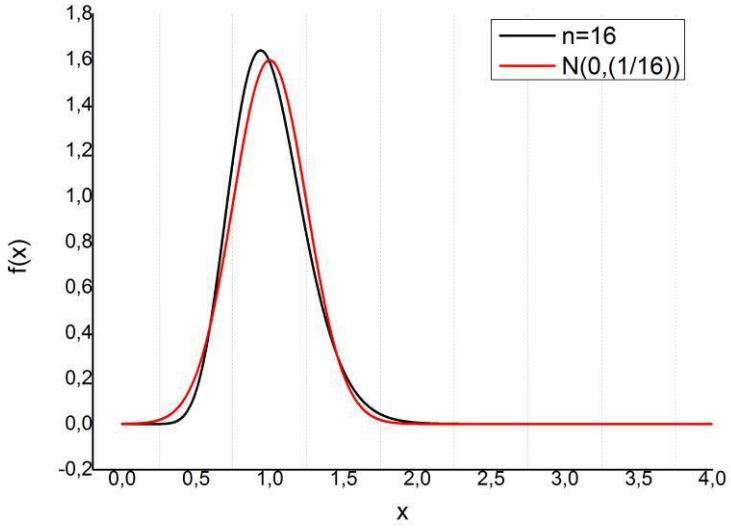

Figure 2.4.2.2 Red line: Normal distribution that has the same mean and variance. Black line: Probability distribution of the summation of n=16 exponential distributions. It is observed clearly to approach normality.

It is generally the case that, the sample size n increases as the probability distribution of the sample means $\overline{X}$ approaches normality, thereby illustrating the central limit theorem. In practice, the normal approximation becomes much better if sample size gets beyond $n \approx 30$.

In this thesis 19 × SMFs photonic lantern is considered to combine with coherent LIDAR systems. The normal approximation of the photonic lantern becomes very good beyond a sample size of $n = 19$.

2.4.3 Chi-squared Distribution

This section is about the chi-squared distribution that has special part of central limit theorem and provides valuable information for mathematical statisticians, biometricians, economic statisticians and psychologists. We focus just on introducing the basics of the chi-squared and non-central chi-squared distributions to you.

It is also known chi-square and often denoted by χ^2-distribution, each one specified by a parameter called the degrees of freedom of *k*, is the distribution of a sum of the squares of *k* independent standard normal random variables that have a mean of zero and unit-variance Gaussian random variables [61]. The chi-squared distribution changes with the degree of freedom. Figure 2.4.3.1 illustrates several chi-square distributions for different degrees of freedom.

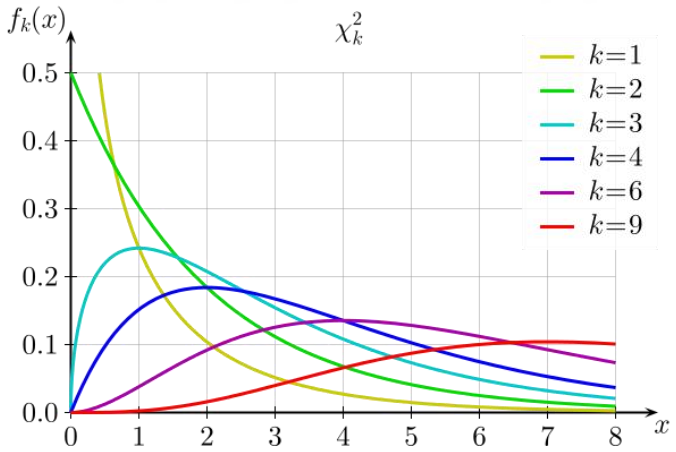

Figure 2.4.3.1 Chi-square distributions changes respectively different *k* degrees of freedom [62].

Lets X_1, ..., X_k are independent, standard normal random variables with zero means and unit-variance , then the sum of their squares;

$$Q = \sum_{i=1}^{k} X_i^2 \qquad (2.4.3.1)$$

is distributed with k degrees of freedom according to the chi-squared distribution. This is often denoted as;

$$Q \approx \chi 2(\mathrm{k}) \text{ or } Q \approx \ \chi 2_{\mathrm{k}} \qquad (2.4.3.2)$$

The chi-squared distribution has one parameter of *k*, a positive integer that specifies the number of degrees of freedom. The chi-squared distribution is actually a simple special case of the non-central chi-square distribution. One way to generate random numbers with a $\chi 2$ distribution (with *k* degrees of freedom) is to sum the squares of *k* standard normal random numbers that has a mean equal to zero. What if the normally distributed variables have a mean other than zero? The sum of squares of these numbers provides the non-central chi-square distribution. The non-central chi-square distribution requires two parameters: the degrees of freedom of *k* and the non-centrality parameter of λ. The non-centrality parameter is the sum of the squared means of the normally distributed quantities. Figure 2.4.3.2 illustrates several non-central chi-square distributions for different degrees of freedom of *k* and non-centrality parameter of λ.

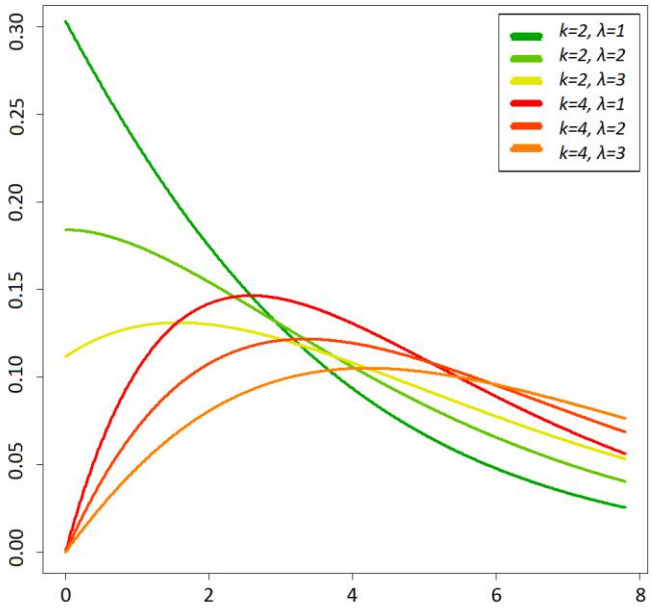

Figure 2.4.3.2 Non-central chi-square distributions changes respectively different *k* degrees of freedom and non-centrality parameter of λ [63].

Lets X_1, ..., X_k be k independent normally distributed random variables with means μ_i and unit variances, then the sum of their squares is the same Eq 2.4.3.1;

$$Q = \sum_{i=1}^{k} X_i^2 \qquad (2.4.3.3)$$

is distributed according to the non-central chi-squared distribution. The non-centrality parameter is given by;

$$\lambda = \sum_{i=1}^{k} \mu_i^2 \qquad (2.4.3.4)$$

So; if the equation 2.4.3.1 is regenerated to originate given above information, table 2.4.3.1 is formed for $X_i \sim N(\mu_i, \sigma_i^2)$, $i = 1, \cdots, k$ independent random variables;

Table 2.4.3.1 General notation of chi-squared distribution.

Distribution	**Math. Model**
Chi-square distribution	$\chi 2_k = \sum_{i=1}^{k} \left(\frac{X_i - \mu_i}{\sigma_i}\right)^2$
Non-central chi-square distribution	$\chi 2_k = \sum_{i=1}^{k} \left(\frac{X_i}{\sigma_i}\right)^2$

2.5 Design Architectures

This section gives a detailed description of photonic lantern based coherent LIDAR receiver processing and describes the LIDAR equation, which can be used to anticipate the performance of a LIDAR architecture. Free space optical systems have two main parts, transmitter and receiver. Transmitter part is generally simple and similar. Although the transmitter design is relatively straightforward, the system performance is mainly determined by the receiver part. So, we have focused on an alternative modeling coherent LIDAR system that is based on photonic lantern to redesign receiver part of the identical coherent LIDAR system. Through this alternative model, our results show that using photonic lanterns the detection ratio has improved. The results are compared with a standard coherent LIDAR receiver, which shows the effectiveness of photonic lantern based.

3D light detection and ranging (LIDAR) systems have many applications such as surveying, terrain mapping, robotics, meteorology, wind analysis and

autonomous navigation [21], [37]. This system has different detection systems depending on the application ranging. Coherent detection based LIDAR systems have the potential to provide quantum noise limited performance[64]. However coherent systems suffer from poor free space to fiber collection efficiency due to the single mode characteristics and small size of the optical fiber.

In order to overcome this problem photonic lanterns are introduced to effectively collect the multimode beam coming from free space and convert it to a number of SMFs [39]. Using the photonic lanterns a free space to single mode efficiency improvement of 8 dB is obtained relative to standard SMFs for near field distances. The photonic lantern is shown in a coherent LIDAR system with a voltage signal to noise improvement of 2.8 when compared to standard single mode receivers [39].

Herein, this thesis presents a method of improving the bit error rate of coherent LIDAR receiver system using a *photonic lantern*. In order to achieve this, we investigated the *photonic lantern* properties for *coherent* LIDAR receiver architectures. We reach some numerical results for the bit error rate improvement of photonic lantern based coherent receivers. The results show that the detection ratio of the coherent receiver is improved to % 95 from % 70 when using 19-port photonic lantern and optic pulse power is taken as 400 mW.

2.5.1 Coherent detection modeling

Coherent LIDAR system has been discussed to analyze bit error rate of coherent receiver systems. A schematic representation of the coherent LIDAR system is shown in figure 2.5.1.1.

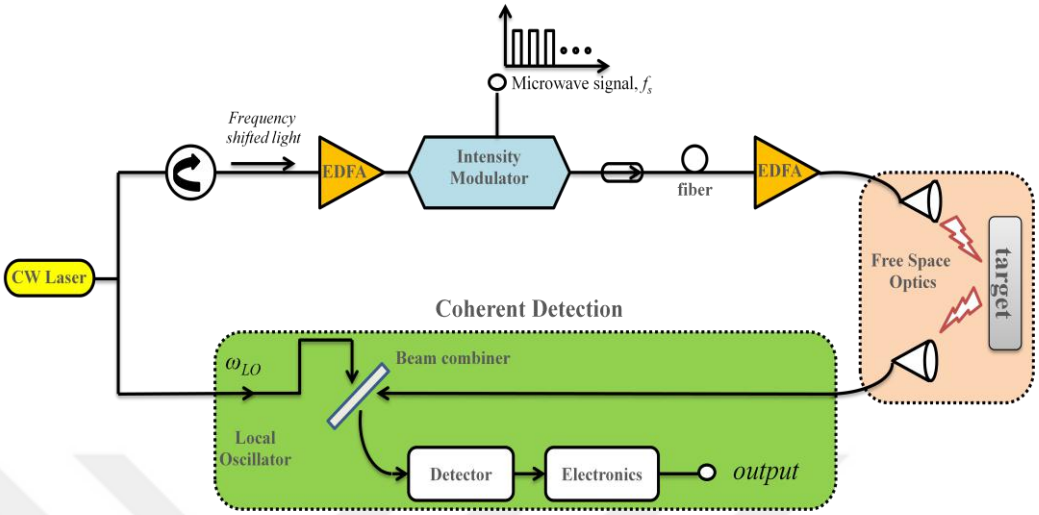

Figure 2.5.1.1 Schematic illustration of a coherent detection scheme.

The primary difference from incoherent systems is that in the coherent receiver a part of the output laser signal is split off and redirected to the coherent detection part. This laser signal is then aligned with that reflected signal from target, and the coherent detection then operates as a mixer to combine the optical signal coherently with a continuous-wave (CW) laser signal before falling on the detector. The CW laser signal is generated from *local oscillator* (LO) to improve the performance of detection. To analyze how mixing of the LO output with the received optical signal, the received optical field can be written as [65];

$$E_s = A_s \exp\left[-i(\omega_0 + \phi_s)\right] \tag{2.5.1.1}$$

where ω_0 is the carrier frequency, A_s is the amplitude, and ϕ_s is the phase. The output of LO can be written by a similar expression[65],

$$E_{LO} = A_{LO} \exp\left[-i(\omega_{LO} + \phi_{LO})\right] \tag{2.5.1.2}$$

where ω_{LO}, A_{LO} and ϕ_{LO} represent the frequency, amplitude and phase of the LO, respectively. After photo detector that generates a current that changes as a function of the intensity of incident optical light, the output current $i(t)$ of single mode coherent detection can be written approximately as;

$$i(t) \approx \eta_S \left(\sqrt{P_{LO}} \cos(\omega_{LO} t) + \sqrt{P_S} \cdot \cos(\omega_S t + \phi) \right)^2 \qquad (2.5.1.3)$$

where ω_{LO} is the optical frequency of the local oscillator (LO), η_s is a receiver loss and gain factor, ϕ is the relative phase between the signal and LO due to the Doppler effect. It is faced with three terms when this equation is solved. A constant term + high frequency term + $\left(\sqrt{P_{LO}} \sqrt{P_S} \cdot \cos[(\omega_S - \omega_{LO})t + \phi] \right)$. Since $P_{LO} \gg P_S$ in practice, first term is direct current (DC) in electrical domain, it does not contain any information. Second term can be removed using filter. The single mode coherent detection current is then given by the third term" $\left(\sqrt{P_{LO}} \sqrt{P_S} \cdot \cos[(\omega_S - \omega_{LO})t + \phi] \right)$" that consists of alternating-current (AC) in equation 2.5.1.3. As shown this equation, the AC signal amplitude is proportional with the square root of the LO field and optical signal radiation received from free space.

Photonic lantern has been used by Leon-Saval *et al*. to enable the high performance of SMF devices to be attained in multimode fibers. It is known that signals incoming from free space are multimode form. The photonic lantern can collect light into multimode fiber and transmit it to an array of SMFs. Transmission loss that occurs between multimode and SMFs has been analyzed by Noordegraafet *et al.* for 19 and 61 port photonic lanterns and it has resulted with low loss behavior. A similar study has been also executed by Birks *et al.* using 120 port photonic lantern. In this chapter, we have focused the 19 port photonic lantern and compare it to bit error rate performance of an individual SMF under same conditions. So, we have designed two LIDAR receiver architectures which include single-mode coherent receiver and lantern-based coherent receiver. The first architecture uses a SMF to collect the reflected optical field after the receiver sensor. The optical signal is mixed with a local oscillator, and sent to a photo detector. This architecture is well known as a typical coherent LIDAR system, as shown in figure 2.5.1.2 (a).

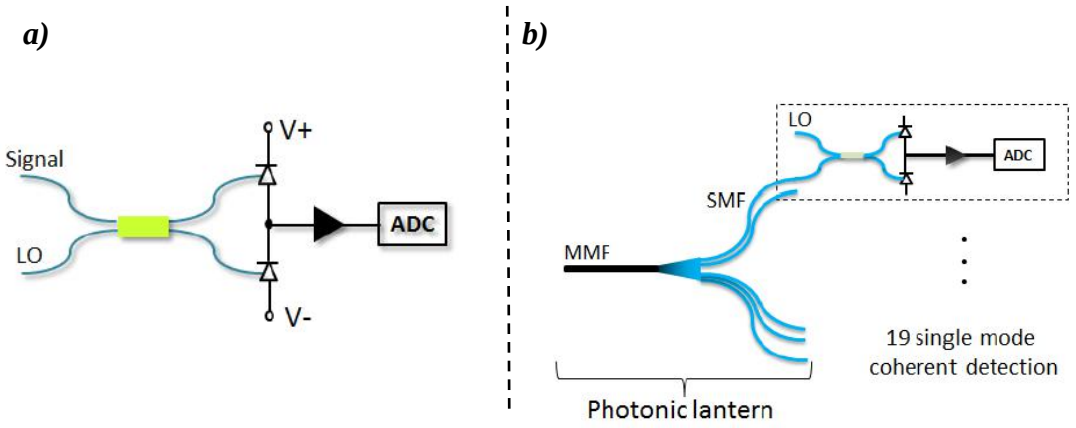

Figure 2.5.1.2 Architectures of detection system for SMF (a) and photonic lantern (b) based coherent systems [39]

The second architecture coherent LIDAR receiver system has a photonic lantern for collection, as shown in figure 2.5.1.2 (b). It is a device that made by tapering a bundle of 19 several relatively small SMFs. It allows low-loss optical waveguide through its feature that collects light in a large core multimode fiber and converts to N × SMFs. Each SMF of the photonic lantern is merged with single-mode local oscillator using an optical coupler and sent to a photo detector. This method has been reprocessed for each single-mode part one by one and then 19 channel SMFs have been combined to get average.

We should struggle to express as a mathematical model step by step. The average value of optical power sent to the target measured easily using an optical power meter. However, the system performance will be determined by optical peak pulse power not the average optical power. Figure 2.5.1.3 shows typical optical peak pulses generated. The optical pulses have a pulse repetition time of Δt_{prt}, and an average optical transmitted power of $P_{tx.avg}$.

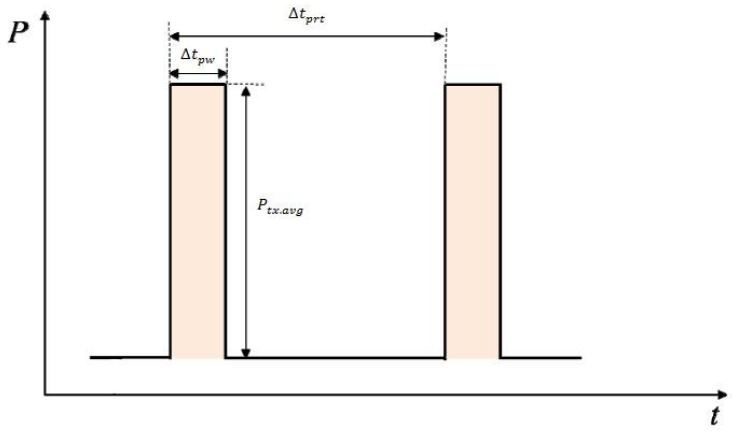

Figure 2.5.1.3 Illustration of optical pulse power generated.

The transmitted optical pulses have an extinction ratio (ER). Given below equation is used to calculate the optical pulse peak power from the average optical power [57]:

$$P_{tx.pk} = \frac{P_{tx.avg}}{\Delta t_{pw}/\Delta t_{prt} + ER\ (1 - \Delta t_{pw}/\Delta t_{prt})} \qquad (2.5.1.4)$$

where Δt_{pw} is optical pulsewidth duration, Δt_{prt} is pulse repetition time. Our reference laser source has a narrow linewidth (~1 kHz) and centered at 1550nm. Extinction ratio is one of the most important parameter that determines the pulse peak power at a given average power. The extinction ratio expresses how much power is transmitted effectively. In the absence of adequate extinction ratio, the sum of the optical pulse peak power between two optical pulses can be even higher than the optical power transmitted. That's why the high extinction ratio is an important criterion. In ideal case, $\min\ (P_{tx.avg}) = 0$ where the extinction ratio is infinite. It can be expressed in terms of loss, or BER penalty. The power penalty as a function of extinction ratio is graphed in figure 2.5.1.4 for logarithmic (dB) ratios.

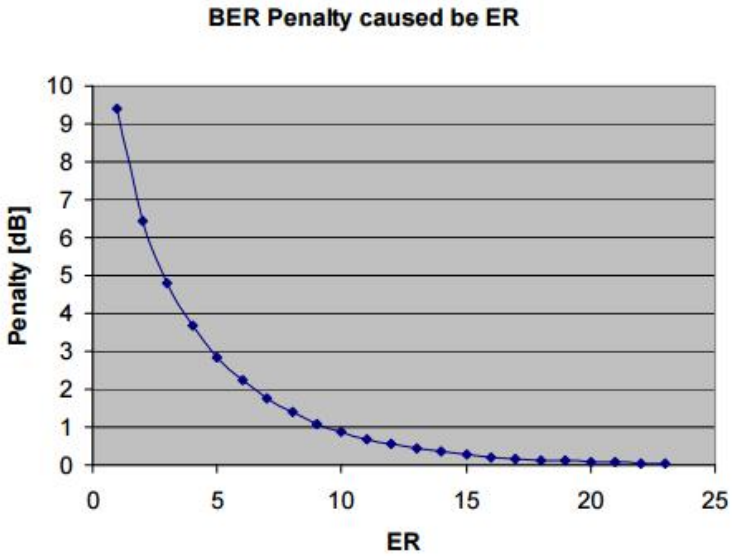

Figure 2.5.1.4 BER penalty vs. extinction ratio *(ER)*

The extinction ratio of a typical electro-optical modulator is about 20 dB, but this can be increased with special design electro-optic modulators. In this thesis, extinction ratio is optimized 20 and 30dB to get desired pulse peak power.

The received signal is proportional to the amount of backscattered light intensity reflected from target and recaptured by the LIDAR focusing lens. Thus, the received signal depends directly on the surface roughness, reflectivity and absorption of target.

Accordingly, the transmission loss is an essential basic parameter for our LIDAR system. The transmission loss calculation looks at the path loss itself and contains other factors relating to average reflectivity, waist diameter of lens, distance of located target and solid angle of Lambertian. In these circumstances, there is no obstacle that might cause the signal to be refracted, or that might cause additional attenuation. In this thesis, reflectivity of target has been calculated to be 30% ($\eta_{tg} \approx 0.3$) and solid angle has been accepted solid angle of Lambertian ($\Omega_{tg} = \pi$) which are same value of reference [57]. With all of

these parameters, the total round-trip optical channel loss rate in LIDAR system uses wide area (mult-mode) detector:

$$\eta_{ch} = \frac{\eta_{tg} D^2 \pi}{4 L_{tg}^2 \Omega} \qquad (2.5.1.5)$$

where D is waist diameter of lens, L_{tg} is distance and Ω is solid angle.

This channel loss is ideal and working quite well for wide area detectors but; we need a correction function to multiply with channel loss equation for SMF based LIDAR systems. The reason of this, the waist diameter of backscattered image signal is greater than SMF optic cable. This circumstance is illustrated in figure 2.5.1.5.

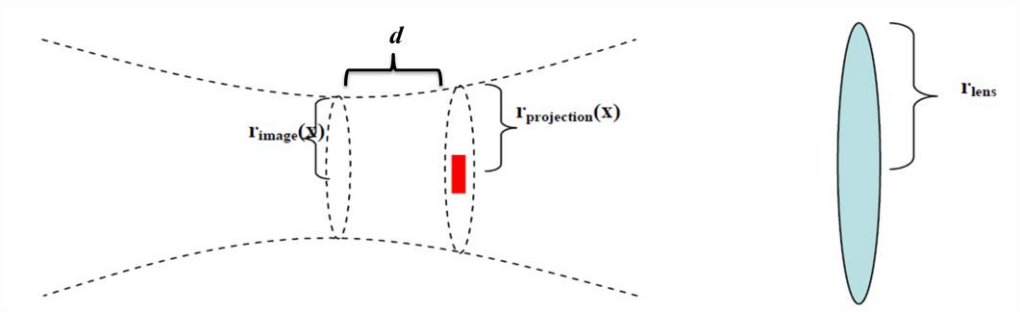

Figure 2.5.1.5 Description of optic system on detector side [copyright from reference 25]

If the target is far away according to Fraunhofer distance ($2D^2/\lambda$, where D is diameter of lens, λ is wavelength), LIDAR can focus on the target and all backscattered light fall on the fiber optic cable. However, in near field, we are getting across the situation of figure 2.5.1.5. Red mark represents fiber optic cable. $r_{projection}(x)$ describes the diameter of backscattered image signal. A collection efficiency of a LIDAR system has been introduced by Sonnenschein[66], backscattered signal is compared with a reference beam. When the collection efficiency function ($F_{collect}(x)$) is modeled, a Cauchy

distribution centered around the focus distance. It describes the amount of backscattered light that is reached to receiver lens of LIDAR. $F_{collect}$ is determined below:

$$F_{collect} = \frac{A_{fiber}}{A_{projection}} \tag{2.5.1.6}$$

where A_{fiber} is area of fiber optic cable, $A_{projection}$ is area of backscattered image signal. To calculate $A_{projection}$, below equations are used:

$$A_{projection} = \pi {r^2}_{projection}$$

$$ {r^2}_{projection} = {r^2}_{image}\left[1 + \left(\frac{\lambda d}{\pi {r^2}_{image}}\right)^2\right] \tag{2.5.1.7}$$

where d is a distance of between fiber and image, r_{image} is radius of backscattered image. You can examine the reference [25] for more detailed calculations.

2.5.2 Compare detection architectures

Data stream Results:

This thesis proposes and compares two detection architecture performances model of LIDAR systems that are SMF based and photonic lantern based. The coherent detection models for both architectures are shown in figure 2.5.2.1(a) and (b). Using the transmitted beam average power (P_{tx}) and the link loss parameters, the received optical beam power (P_{rx}) is calculated and is mixed with the local oscillator (having a power P_{LO}) on the photo detector. The photo

detector has a responsivity of *R*. The detected photocurrent is squared in order to obtain a variable which is proportional to the light intensity.

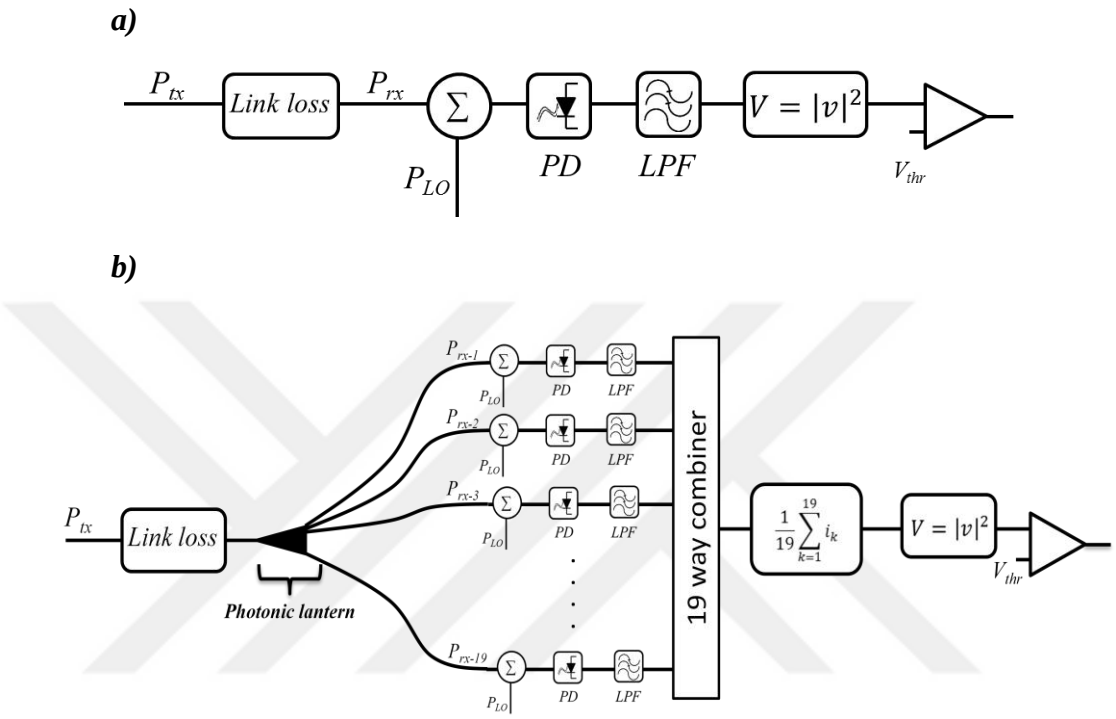

Figure 2.5.2.1 Architectures of detection systems for SMF (a) and photonic lantern (b) based coherent systems

Figure 2.5.2.1(a) shows a standard coherent detection setup where the received optical signal is combined with a local oscillator. Figure 2.5.2.1(b) shows a coherent detection system using a photonic lantern. Using the photonic lantern, multimode optical signal is collected from the free space and distributed to 19 SMFs. The photodetected signal from the 19 channels will be combined and after the squaring, they will be averaged. We assume the noise is limited with shot noise only or shot + TIA noise. The TIA and shot noise is represented as Gaussian process. The transimpedance gain is equal to 500W, and the TIA noise figure is assumed to be approximately 3dB based on measurements of noise statistics and the temperature is assumed to be 333K maximum temperature limit for workplace.

Also, link loss versus target distance relationships is given figure 2.5.2.2. In near field (0~100m) there is almost constant value of link loss, which is equal to around -92 ~ -93dB.

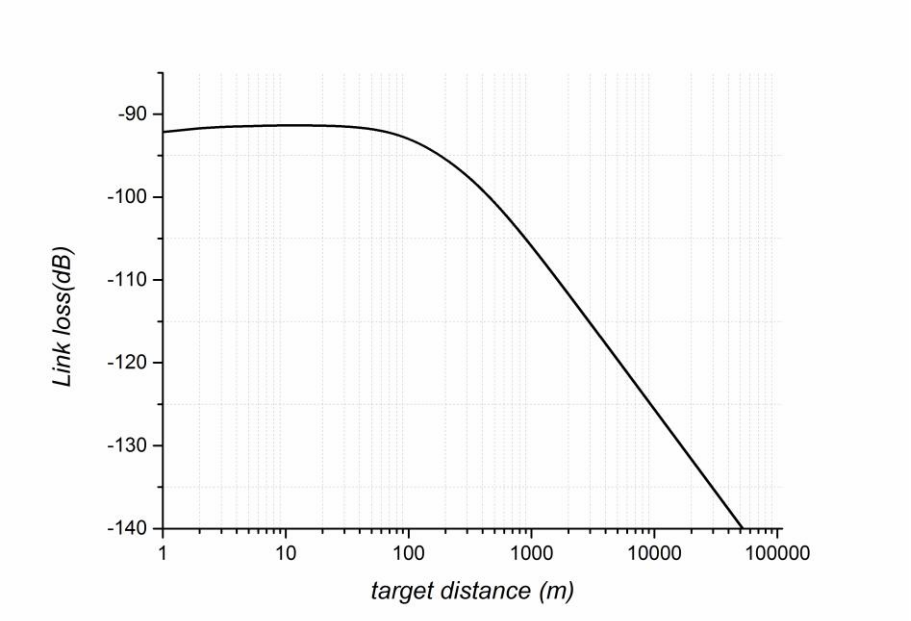

Figure 2.5.2.2 The total optical loss of coherent LIDAR detection.

In the modeling the peak transmitted optical power is taken as the values in the table 2.5.2.1 and tried various variations. The link loss is calculated using the method given in reference [25] and found as ~92.99dB for a distance of 100 meters and for a diffuse target reflectivity of 0.3. The photo detector responsivity is taken as 0.8 and the bandwidth of the photodetected signal is limited to 2 GHz. The optical power of the local oscillator is assumed to be 10 mW as the typical maximum optical input power for the photodetectors are around 20 nW. The optical pulse width and the pulse repetition rate are taken as 10 ns and 10 kHz respectively.

Table 2.5.2.1 Parameters of coherent LIDAR systems.

Wavelength	1550nm
Average optical power	125,200,250,300,400 and 500mW
Distance between fiber and lens	10cm
Extinction ratio	20 and 30dB
Target reflectivity	0.3
Radius of fiber	5μm
Angle of reflection, Ω	π, (Lambertian solid angle)
Distance of target	100m

It was shown previously that the optical signal distribution of the 19 × SMFs of the photonic lantern are random. For the simulation we used the power distribution that is reported in reference [38]. It's also given figure 2.5.2.3 below;

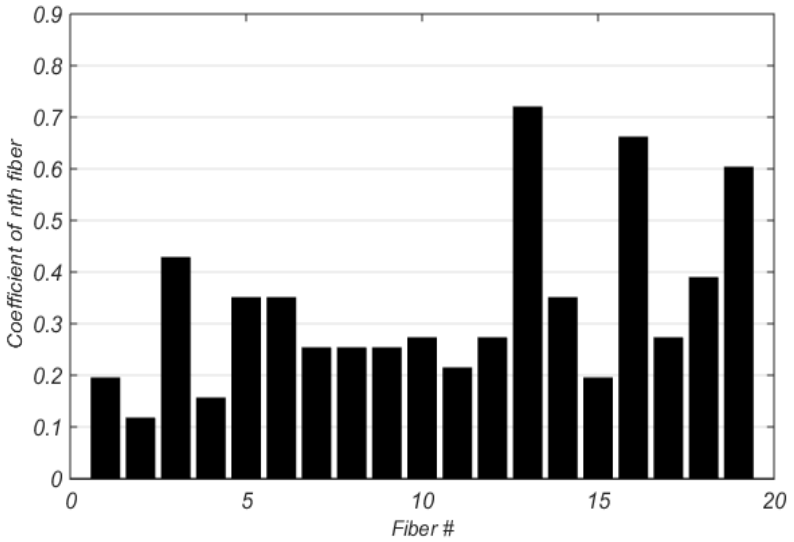

Figure 2.5.2.3 Output signal power distribution of the 19 × SMFs photonic lantern.

19 × SMFs intend to increase the performance of a signal relative to noise that is obscuring it. The signal-to-noise ratio has been increased proportional to square

root of the number of SMFs by photonic lantern$\left(\frac{SNR}{\sqrt{N}}\right)$. This signal processing technique, signal averaging, is applied to both architectures of our coherent LIDAR systems with 500mW and illustrated in figure 2.5.2.4.

a)

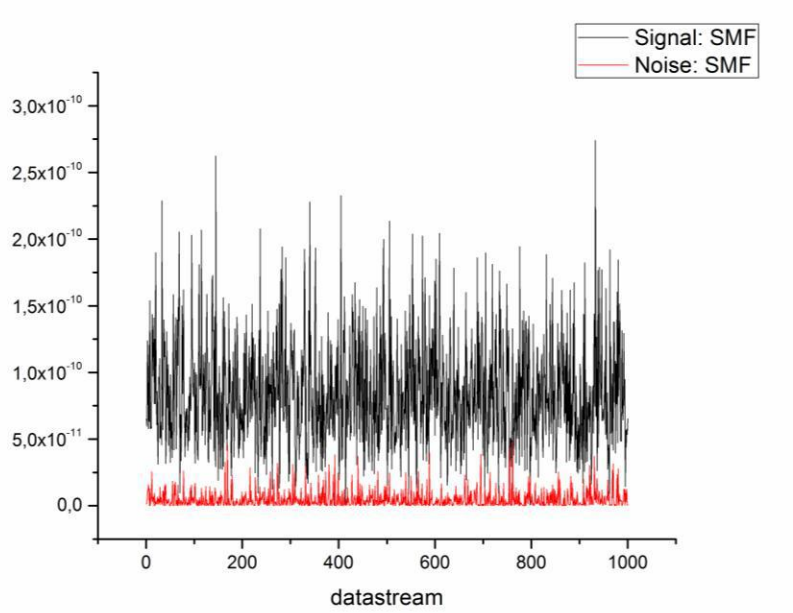

b)

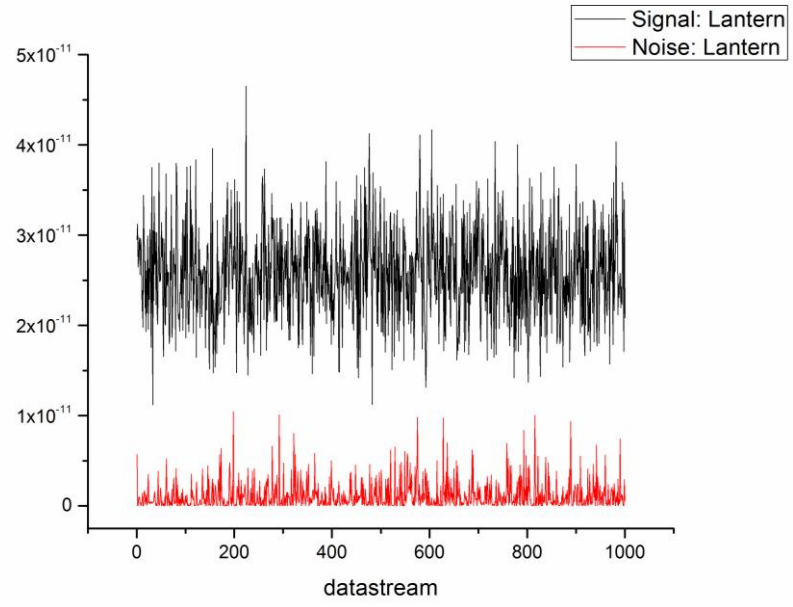

Figure 2.5.2.4 Architectures of detection systems for SMF (a) and photonic lantern (b) based coherent systems

BER Results:

All electrical signals of 19 × SMF collected in phase coherency and so amplitude of output signal will increase, but noise will be self-suppress because it has Gaussian random distribution. As it has been pointed out that desired signal is virtually distinguishable from the unwanted noise according to result of figure 2.5.2.4 (b). This SNR improvement has also affected to bit error rate performance positively. The bit error rate is calculated using the following equation.

$$\text{BER} = p(signal)P[noise|\, signal] + p(noise)P[signal|\, noise] \qquad (2.5.2.1)$$

where *p(x)* is the probability of transmitting an x (signal or noise) and *P[x | y]* is the probability of detecting x given that y is sent. The point of decision is taken as the intersection point of the noise and signal plots. Following figure 2.5.2.5 and 2.5.2.6 show probability density functions (PDFs) versus photocurrent statistics graphs of our two coherent LIDAR systems that are SMF based and photonic lantern based for different optical output powers and shot noise only at 20-30dB extinction ratio.

a) ***b)***

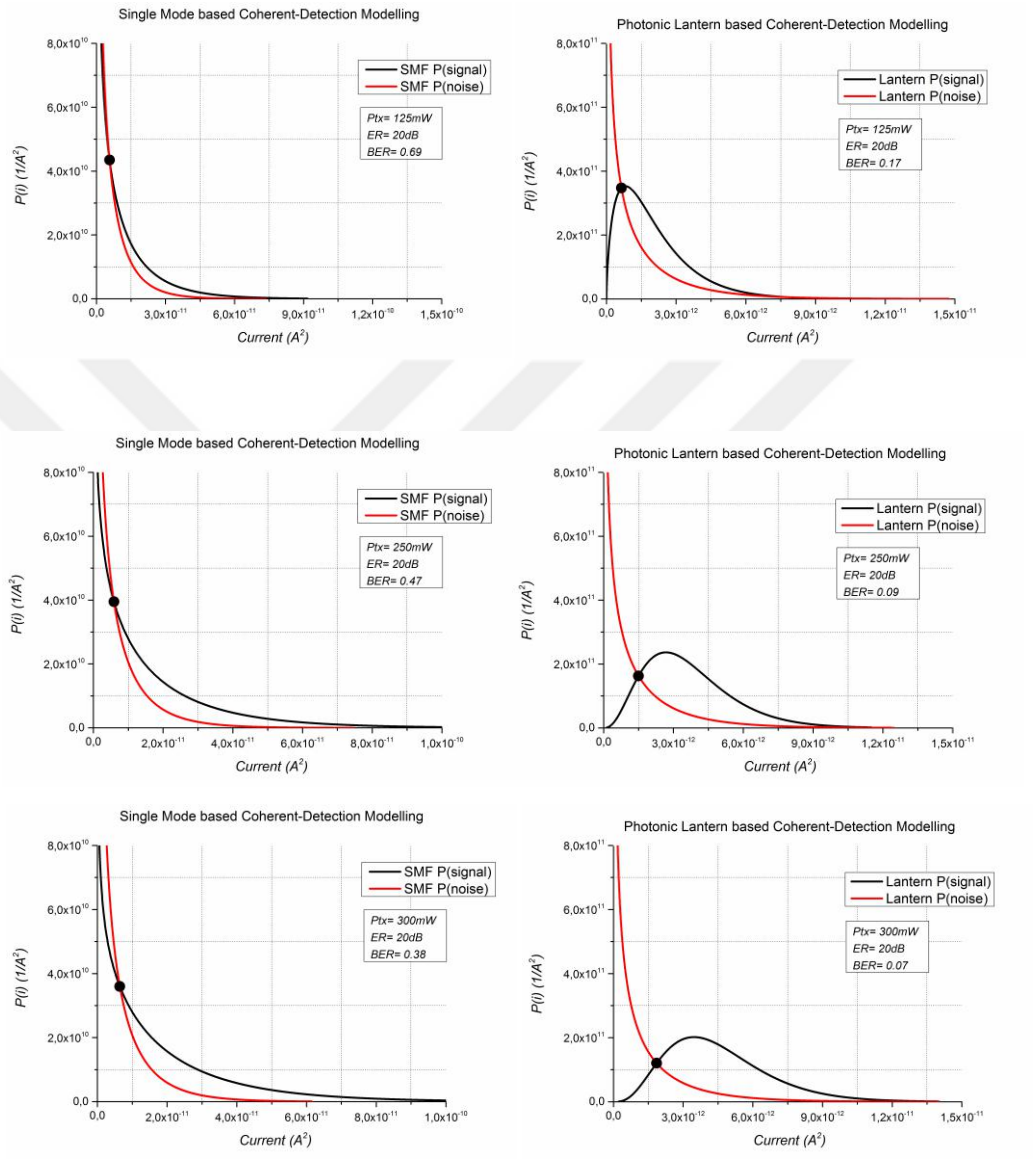

Figure 2.5.2.5 Probability density functions for single mode based receiver (a) and photonic lantern based receiver (b) for 125, 250 and 300mW at 20dB ER.

a) ***b)***

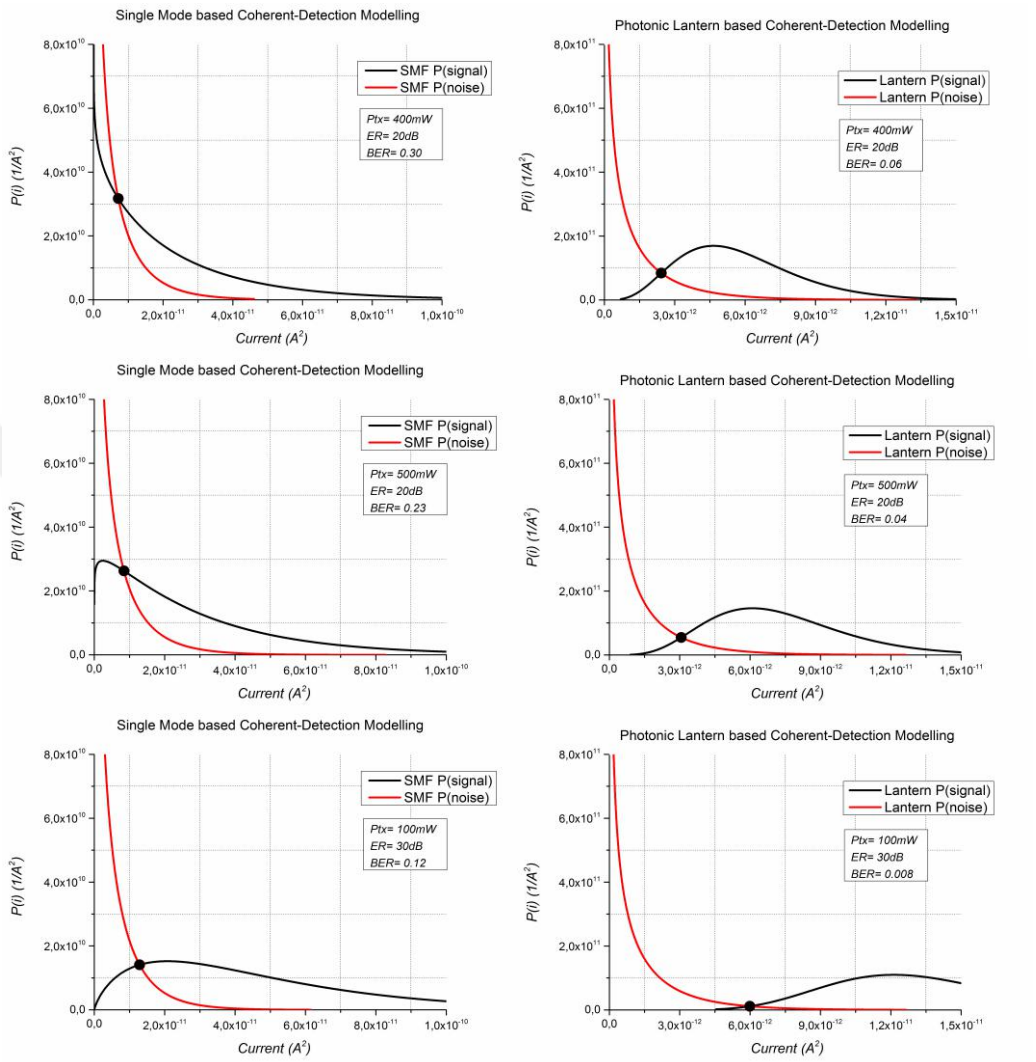

Figure 2.5.2.6 Probability density functions for single mode based receiver (a) and photonic lantern based receiver (b) for 400, 500mW at 20dB ER and 100mW at 30dB ER.

Figure 2.5.2.5 and 2.5.2.6 show the probability density function comparison of two different coherent detection techniques. The BER is improved to 0.09 from 0.47 using the photonic lantern based coherent detection when optical power is 250mW. This improvement is achieved mainly by the noise averaging. Below BER value of 0.1 is acceptable for many commercial systems.

Following figure 2.5.2.7 shows probability density functions (*PDFs*) versus photocurrent statistics graphs of our two coherent LIDAR systems that are SMF based and photonic lantern based for different optical output powers, shot noise and TIA noise at 20dB extinction ratio.

a) ***b)***

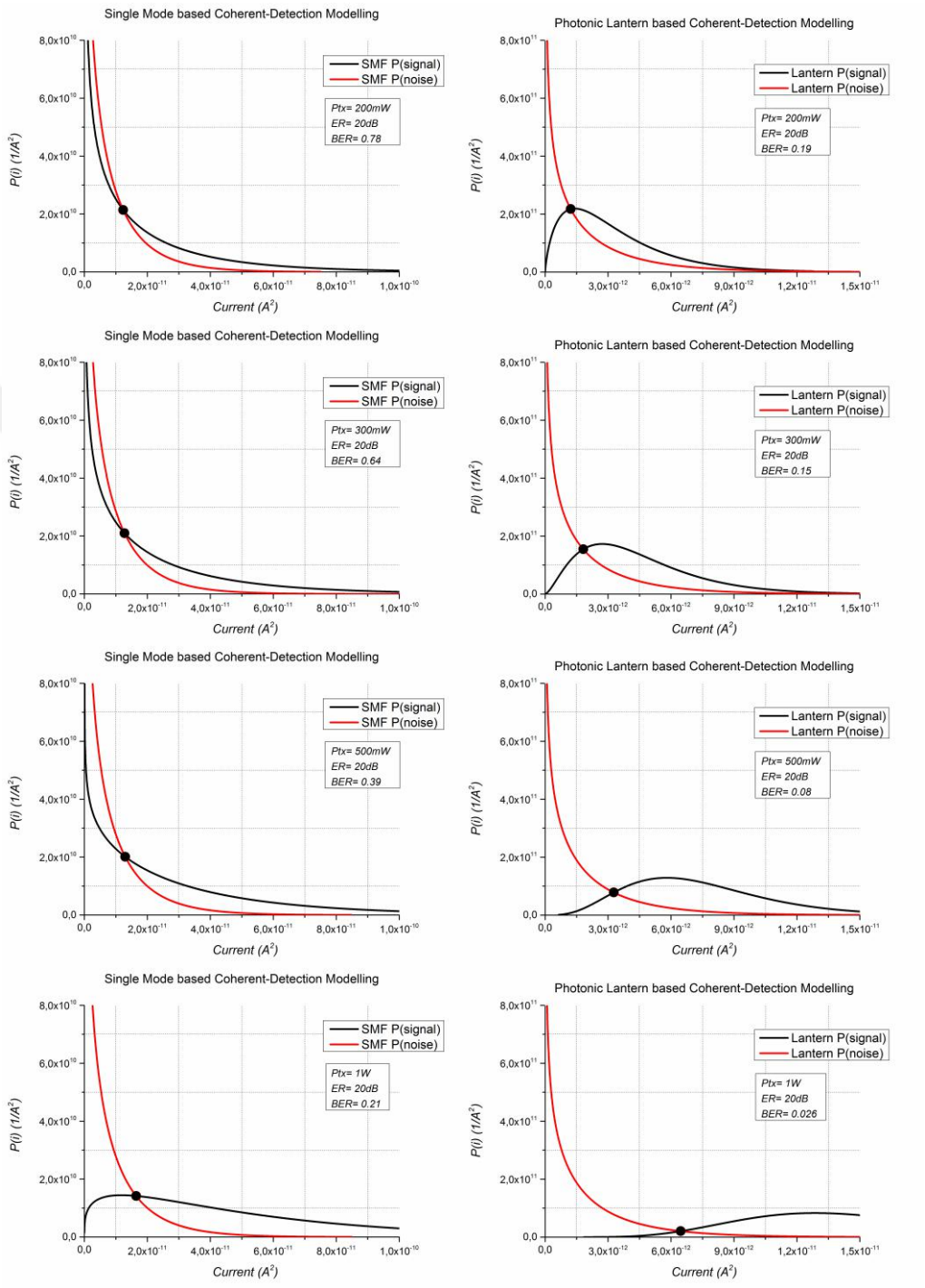

Figure 2.5.2.7 Probability density functions for single mode based receiver (a) and photonic lantern based receiver (b) for 200, 300, 500mW, 1W at 20dB ER, shot+TIA noise.

BER improvement of photonic lantern-based coherent receivers over SMF based coherent receivers is computed and illustrated in figure 2.5.2.5 and 2.5.2.6. Our results show that; using the photonic lantern based coherent LIDAR systems the probability of detection can be increased significantly which can be traded with range and higher detection speeds. The BER is improved by a factor of very huge various coefficients according to optical powers and extinction ratios. These improvements are achieved with using 19 × SMF combined into photonic lantern. The findings are of direct practical relevance that can increase the system performance of LIDAR based on systems for demanding applications.

We know that, the bit error probability *p(signal) and p(noise)* are not equal each other. So, to define minimum BER calculation we don't have to take the intersection point of signal and noise. According to following figure 2.5.2.8, the minimum BER point has remained left side the intersection point previously received. So, if current value of new point is adequate, we can calculate better BER value than the previously computed value.

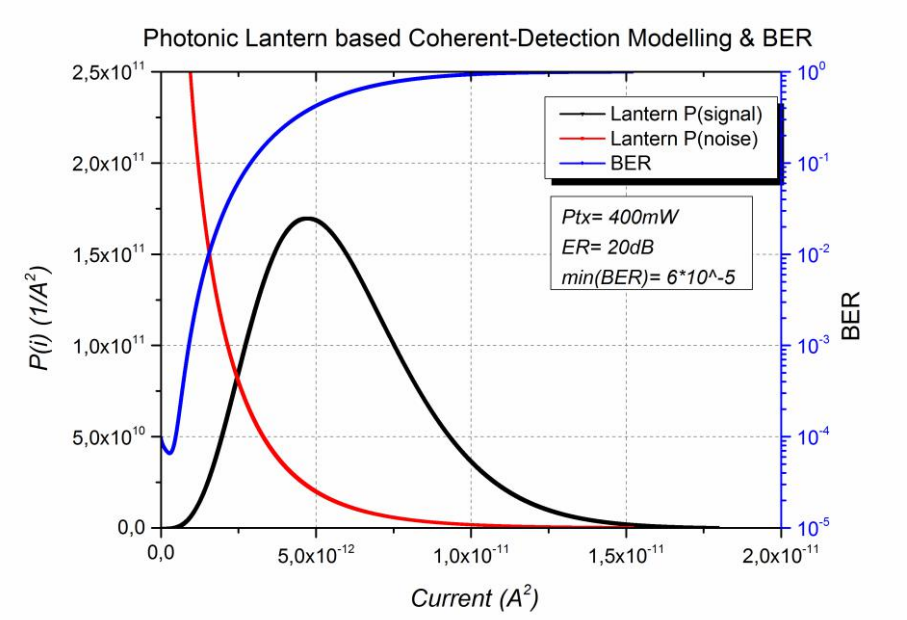

Figure 2.5.2.8 Minimum BER calculation for 400mW.

In this thesis has also been observed probability density function of single mode based coherent LIDAR system when optical power increases from 200mW to 1W (figure 2.5.2.9).

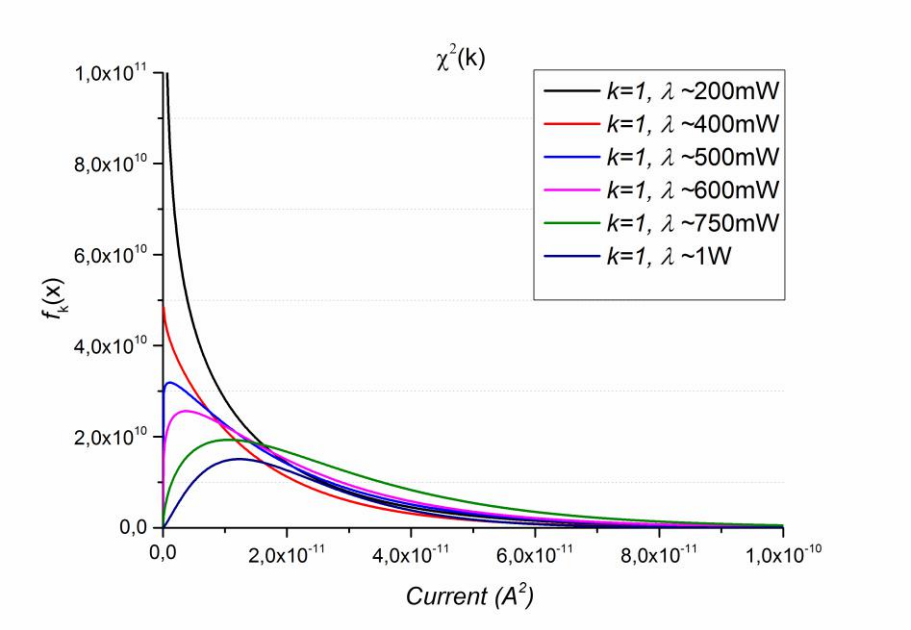

Figure 2.5.2.9 Probability density functions for single mode based receiver for various optical power.

Distributions of figure 2.5.2.9 are exactly same with chi-squared distribution theorem studied in chapter 2.4.3.

Comparison of Numeric and Mathematical Models Results:

- ***For SMF Based LIDAR Systems:***

We also generated mathematical representations or models of our LIDAR architectures. We have reviewed which devices and behaviors can be described. According to our SMF based LIDAR systems, we have explained with following by mathematical description which is illustrated figure 2.5.2.10.

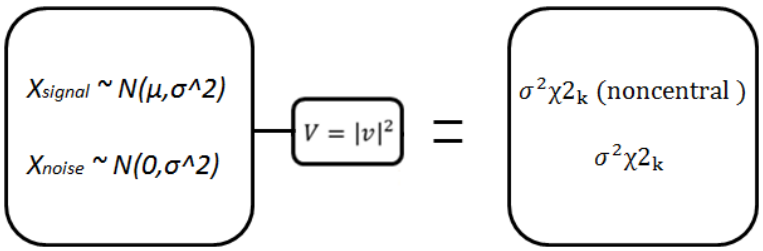

Figure 2.5.2.10 Mathematical modeling that shows how PDFs of signal and noise approach to building a model output PDFs.

SMF based LIDAR systems were simulated and compared based on a projected reach. However, for highest confidence we analyzed two performances for 200, 750mW and 1W comparisons mathematical model and numerical model with MATLAB.

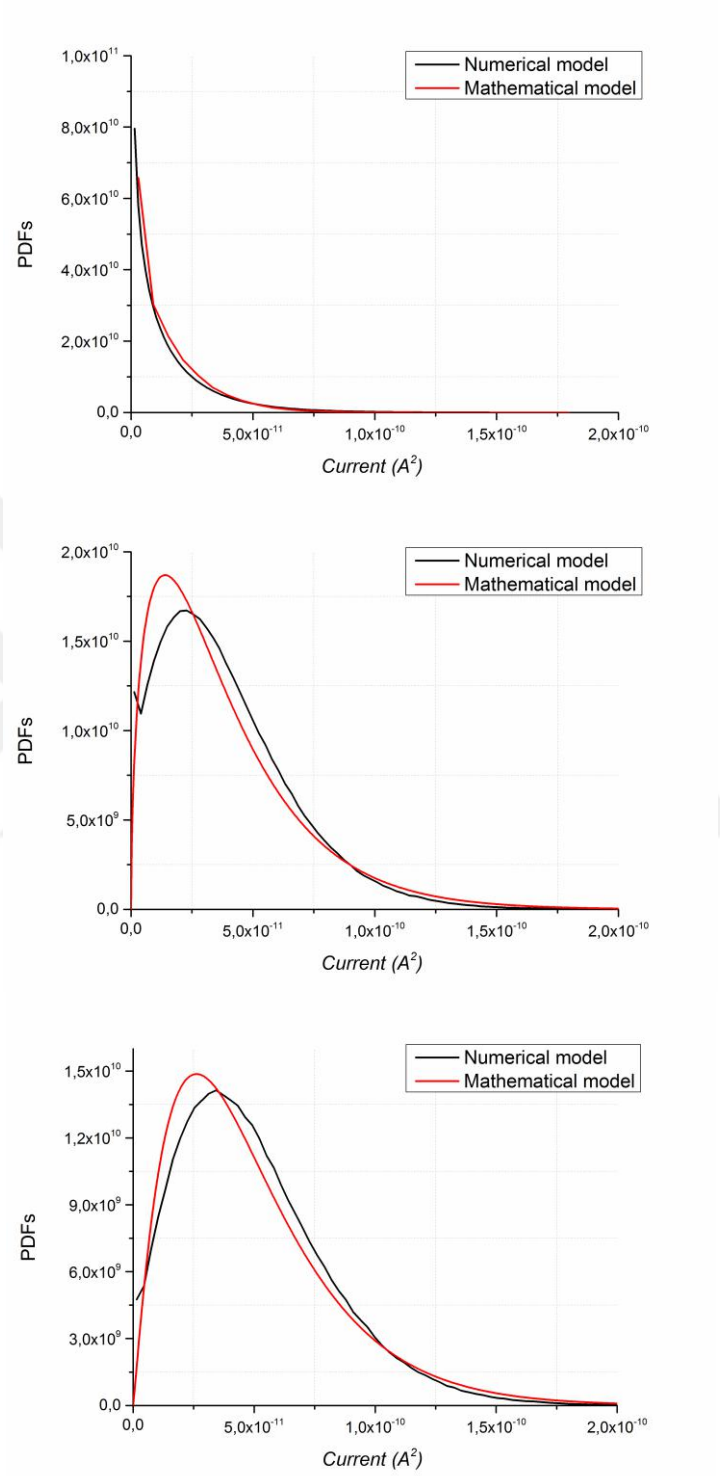

Figure 2.5.2.11 Probability density functions of numerical and mathematical models for single mode based LIDAR receiver for 200,750mW and 1W optical powers respectively.

According to the figure 2.5.2.11, there are two hypotheses that can be made comparison for numerical model: 200mW (data 01) and mathematical model: 200mW (data 02);

• H_0: There is no significant correlation between the data 01 and data 02.
• H_1: There is a significant correlation between the data 01 and data 02.

The returned value of significant = 0,000 < 0,05 indicates that H_0 hypothesis is rejected . As a result, there is a significance correlation statistically between data 01 and data 02 at the %95 confidence interval as represented in the equation below:

$$r_{data01,data02}=0.9935 \qquad (2.5.2.2)$$

- ***For Photonic Lantern Based LIDAR Systems:***

We have repeated this procedure for photonic lantern based coherent LIDAR architecture. We have reached to following mathematical description which is illustrated figure 2.5.2.12.

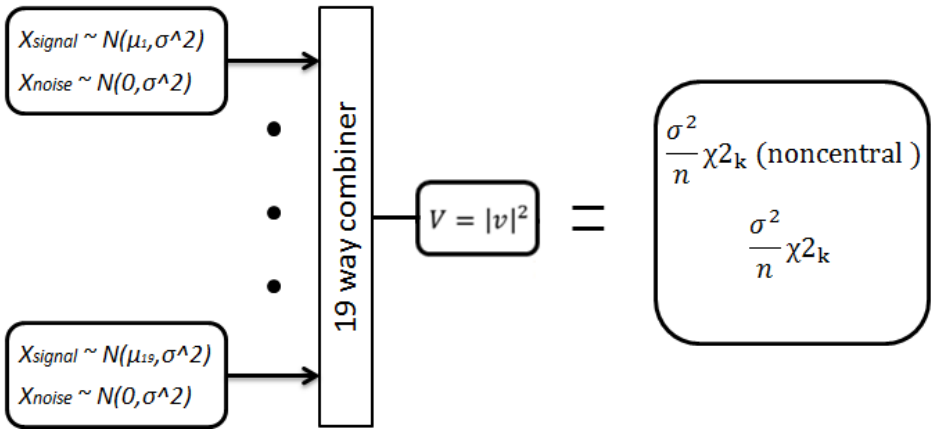

Figure 2.5.2.12 Mathematical modeling that shows how PDFs of signal and noise approach to building a model output PDFs.

Photonic lantern based LIDAR systems were simulated and compared based on a projected reach. However, for highest confidence we analyzed two performances of 200, 750mW and 1W comparisons mathematical model and numerical model with MATLAB.

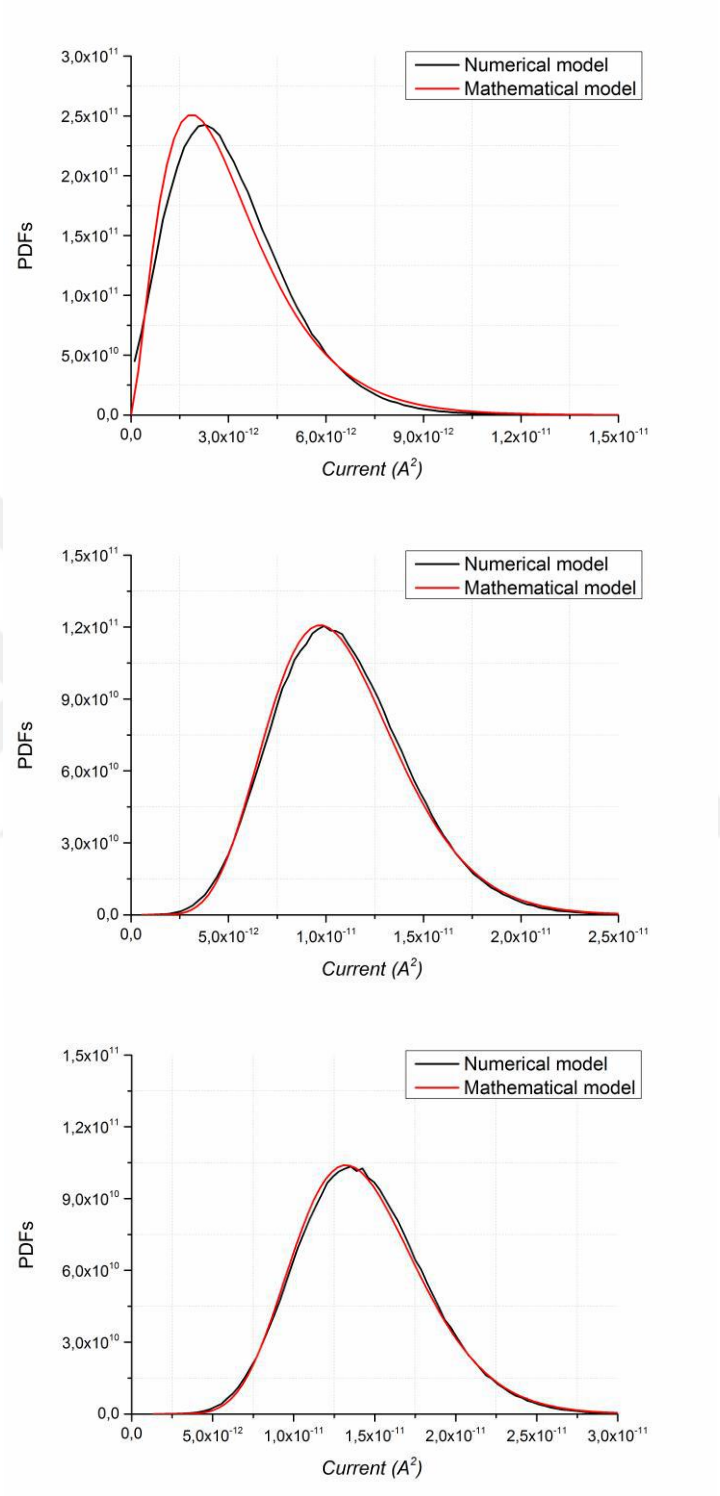

Figure 2.5.2.13 Probability density functions of numerical and mathematical models for photonic lantern based LIDAR receiver for 200, 750mW and 1W optical powers respectively.

According to the figure 2.5.2.13, there are two hypotheses that can be made comparison for numerical model: 750mW (data 03) and mathematical model: 750mW (data 04);

• H_0: There is no significant correlation between the data 03 and data 04.
• H_1: There is a significant correlation between the data 03 and data 04.

The returned value of significant = 0,000 < 0,05 indicates that H_0 hypothesis is rejected . As a result, there is a significance correlation statistically between data 03 and data 04 at the %95 confidence interval as represented in the equation below:

$$r_{data03,data04}=0.9993 \qquad (2.5.2.3)$$

2.6. Remarks

In this part of thesis, bit-error rate improvement of photonic lantern-based coherent receivers over single-mode fiber based coherent receivers is analyzed. The BER is improved with huge factor using the photonic lantern based coherent detection when different optical power and extinction ratio. Our results show that using the photonic lantern based coherent LIDAR systems the probability of detection can be increased significantly which can be traded with range and higher detection speeds.

Chapter 3

Conclusion and Discussion

In the experimental part of this thesis, we developed optical spatial filtering effect for macroscopic imaging and the ratio of scattering photons is decreased to 5 % from 83 %. The limitations of the current LIDAR technology were studied and the problem of the highly scattering in DVF was stated. There was a limitation in our experimental design when broad area photodetector device is operated in DVF. We proposed our solution for the enhancement of the error rate LIDAR system in DVF. For this purpose we demonstrated the concept of LIDAR architectures for SMF and broad area detector. It is experimentally showed significant enhancement in the relative proportion of scattered photons over ballistic photons with 5 % from 83 % improvement in DVF when using SMF.

For mathematical part of this thesis, one of the biggest components used in 3D LIDAR systems is lens diameter. Optical power detection improvement will be found to be 2 when lens diameter is kept $\sqrt{2}$. That means a grateful improvement in the signal to noise ratio, too. But size of optical lens cannot be continually increased in these applications. In this thesis; according to SMF, more optical power has been obtained when using photonic lantern. And this affects the signal to noise ratio which is calculated by improvement of 6. This improvement can be used for higher resolution or faster system.

Free space optical systems require higher performance, as others are lower size, weight and power consumption (SWaP). SWaP systems can be embedded in

micro-nano unmanned aerial systems for reconnaissance, surveillance and intelligence applications such as 3D imaging in limited space environments. If needed, the improvement system performance obtained using photonic lantern can be scarified to design smaller, lighter and less energy consumption of system with same performance as foreseen in thesis. Despite the lens diameter can be decreased, extra components to be added to photonic lantern based LIDAR systems can be seen as increasing the system weight and volume. To solve this problem, the photonic lantern based LIDAR systems must be integrated circuits. When using photonic integrated circuit, present volume and weight will keep less space and weight. This circuit production can cost a little expensive. So; it must be really needs to design photonic lantern based LIDAR system if required higher performance improvement or small size and weight improvement otherwise, it's difficult to verify the increased costs itself. The next phase of the thesis is carried out in real time experimental setup with photonic lantern. To accomplish this, 19-coherent receiver system must be designed and worked simultaneously. It's clear that the cost of this architecture will be high. The rationale for this experiment must be established. The output of this thesis may open the path to experimental demonstration and maybe even to a prototype.

Bit error rate performance of designed photonic lantern based coherent LIDAR system has been also presented in this thesis. Bit error rate has different values in different optical power. Our results show that using photonic lanterns the bit error rate is improved to below 10% from 47% when compared to single mode coherent detection systems under 250 mW optical power.

BIBLIOGRAPHY

[1] Wikipedia, “Engineering Acoustics/Echolocation in Bats and Dolphins.” [Online]. Available: https://en.wikibooks.org/wiki/Engineering_Acoustics/Echolocation_in_Bats_and_Dolphins. [Accessed: 10-Jul-2016].

[2] “How does sonar work?” [Online]. Available: https://www.exploratorium.edu/theworld/sonar/sonar.html. [Accessed: 10-Jul-2016].

[3] R. T. O. T. Report, *Rotary-Wing Brownout Mitigation : Technologies and Training (Remèdes contre le phénomène de brownout*, vol. 323, no. January. 2012.

[4] Booz-Allen-Hamilton, “Ten-year averages from 2002 to 2012 based on nhtsa data,” *US Dep. Transp. - Fed. Highw. Adm.*, 2012.

[5] Wikipedia, “SS Andrea Doria,” 2016. [Online]. Available: https://en.wikipedia.org/wiki/SS_Andrea_Doria. [Accessed: 10-Feb-2016].

[6] Wikipedia, “B-25 Empire State Building crash,” 2016. [Online]. Available: https://en.wikipedia.org/wiki/B-25_Empire_State_Building_crash. [Accessed: 10-Feb-2016].

[7] Wikipedia, “Tenerife airport disaster,” 2016. [Online]. Available: https://en.wikipedia.org/wiki/Tenerife_airport_disaster. [Accessed: 10-Feb-2016].

[8] D. McLeod and J. Jacobson, “Autonomous Inspection using an Underwater 3D LiDAR,” *... , San Diego Mar. ...*, 2013.

[9] J. Fritz, A. J. Gasiewski, and K. Zhang, “3D surface imaging through visual obscurants using a sub-THz radar,” vol. 9087, p. 908702, 2014.

[10] B. Sykora, “BAE Systems Brownout landing aid system technology (BLAST) system overview and flight test results,” pp. 1–15, 2009.

[11] R. D. Visual and E. Solution, “Enhanced Vision Solution for Degraded Visual Environment Enhanced Vision Solution for Degraded Visual Environment.”

[12] E. Trickey, P. Church, and X. Cao, “Characterization of the OPAL obscurant penetrating LiDAR in various degraded visual environments,” *Proc. SPIE*, vol. 8737, no. 613, p. 87370E–87370E–9, 2013.

[13] J. T. Murray, J. Seely, J. Plath, E. Gotfreson, J. Engel, B. Ryder, N. Van Lieu, R. Goodwin, T. Wagner, G. Fetzer, N. Kridler, C. Melancon, K. Panici, and A. Mitchell, “Dust-Penetrating (DUSPEN) ‘see-through’ lidar for helicopter situational awareness in DVE,” vol. 8737, p. 87370H–

87370H–8, 2013.

[14] T. E. Dillon, C. a. Schuetz, R. D. Martin, D. G. Mackrides, S. Shi, P. Yao, K. Shreve, C. Harrity, and D. W. Prather, “Passive, real-time millimeter wave imaging for degraded visual environment mitigation,” vol. 9471, p. 947103, 2015.

[15] Wikipedia, “Lidar.” [Online]. Available: https://en.wikipedia.org/wiki/Lidar. [Accessed: 10-Feb-2016].

[16] Wikipedia, “Google self-driving car.” [Online]. Available: https://en.wikipedia.org/wiki/Google_self-driving_car. [Accessed: 10-Feb-2016].

[17] H. U. Schnitzler and O. W. Henson, Jr., *Performance of airborne animal sonar systems: I. Microchiroptera*. New York: Plenum Press, 1980.

[18] M. A. Richards, J. A. Scheer, and W. A. Holm, *Principles of Modern Radar*. SciTech Publishing, 2010.

[19] J. Ring, “The Laser in Astronomy,” *New Sci.*, vol. 344, pp. 672–673, 1963.

[20] C. Weitkamp, *Lidar : range-resolved optical remote sensing of the atmosphere*, no. 102. 2005.

[21] P. F. McManamon, “Errata: Review of ladar: a historic, yet emerging, sensor technology with rich phenomenology,” *Opt. Eng.*, vol. 51, no. 8, p. 089801, 2012.

[22] O. Mew and B. E. Ambientales, “Maestría en Aplicaciones Espaciales de Alerta y Respuesta Temprana a Emergencias,” 2014.

[23] “United States Department of Agriculture Agricultural Research Service.” [Online]. Available: http://www.ars.usda.gov/main/main.htm. [Accessed: 14-Jul-2016].

[24] FEMA, “Guidelines and Specifications for Flood Hazard Mapping Partners [February 2007]. D.2.8 Wave Runup and Overtopping.,” no. February, pp. 1–31, 2007.

[25] P. Lindelöw, “Fiber Based Coherent Lidars for Remote Wind Sensing,” no. November, 2007.

[26] R. D. Richmond, S. C. Cain, and SPIE (Society), *Direct-detection LADAR systems*. SPIE Press, 2010.

[27] G. Vosselman and H.-G. Maas, “Airborne and Terrestrial Laser Scanning,” *Current*, vol. XXXVI, no. 6 Pt 2. p. 318, 2010.

[28] M. Jawad A. Salehi, Babak M. Ghaffari and M. D., *Advanced Optical Wireless Communication Systems*. 2012.

[29] A. M. Bronstein, M. M. Bronstein, and R. O. N. Kimmel, “Three-Dimensional Face Recognition,” vol. 64, no. 1, pp. 5–30, 2005.

[30] R. Rachmani, A. Zilberman, and S. Arnon, “Computer backplane with

free space optical links: Air turbulence effects," *J. Light. Technol.*, vol. 30, no. 1, pp. 156–162, 2012.

[31] N. Chiodo, K. Djerroud, O. Acef, A. Clairon, and P. Wolf, "Lasers for coherent optical satellite links with large dynamics," *Appl. Opt.*, vol. 52, no. 30, pp. 7342–7351, 2013.

[32] K. Anderson and K. J. Gaston, "Lightweight unmanned aerial vehicles will revolutionize spatial ecology," *Front. Ecol. Environ.*, vol. 11, no. 3, pp. 138–146, 2013.

[33] G. Li, "Recent advances in coherent optical communication," *Adv. Opt. Photonics*, vol. 1, no. 2, p. 279, Apr. 2009.

[34] M. DaneshPanah, B. Javidi, and E. a Watson, "Three dimensional object recognition with photon counting imagery in the presence of noise.," *Opt. Express*, vol. 18, no. 25, pp. 26450–60, 2010.

[35] "Thorlabs.com - Precision Pinholes." [Online]. Available: http://www.thorlabs.de/NewGroupPage9_PF.cfm?Guide=10&Category_ID=22&ObjectGroup_ID=1400. [Accessed: 08-Feb-2016].

[36] K. Shi, P. Li, S. Yin, and Z. Liu, "Chromatic confocal microscopy using supercontinuum light," *Opt. Express*, vol. 12, no. 10, p. 2096, 2004.

[37] P. Toliver, I. Ozdur, A. Agarwal, and T. K. Woodward, "Comparison of LIDAR system performance for alternative single-mode receiver architectures: modeling and experimental validation," in *Proceedings of SPIE - The International Society for Optical Engineering*, 2013, vol. 8731, p. 87310W.

[38] I. Ozdur, P. Toliver, A. Agarwal, and T. K. Woodward, "Free-space to single-mode collection efficiency enhancement using photonic lanterns.," *Opt. Lett.*, vol. 38, no. 18, pp. 3554–7, Sep. 2013.

[39] I. Ozdur, P. Toliver, and T. K. Woodward, "Photonic-lantern-based coherent LIDAR system," *Opt. Express*, vol. 23, no. 4, p. 5312, 2015.

[40] C. Lu and Y. Cui, "Fiber bragg grating spectra in multimode optical fibers," *J. Light. Technol.*, vol. 24, no. 1, pp. 598–604, 2006.

[41] S. G. Leon-Saval, A. Argyros, and J. Bland-Hawthorn, "Photonic lanterns: a study of light propagation in multimode to single-mode converters.," *Opt. Express*, vol. 18, no. 8, pp. 8430–9, Apr. 2010.

[42] D. Noordegraaf, P. M. W. Skovgaard, M. D. Maack, J. Bland-Hawthorn, R. Haynes, and J. Laegsgaard, "Multi-mode to single-mode conversion in a 61 port Photonic Lantern.," *Opt. Express*, vol. 18, no. 5, pp. 4673–8, Mar. 2010.

[43] D. Noordegraaf, P. M. W. Skovgaard, R. H. Sandberg, M. D. Maack, J. Bland-Hawthorn, J. S. Lawrence, and J. Lægsgaard, "Nineteen-port photonic lantern with multimode delivery fiber.," *Opt. Lett.*, vol. 37, no. 4, pp. 452–4, Feb. 2012.

[44] B. Ercan, R. Ryf, J. Bland-Hawthorn, J. R. S. Gil, S. G. Leon-Saval, and N. K. Fontaine, “Mode-selective dissimilar fiber photonic-lantern spatial multiplexers for few-mode fiber,” *39th Eur. Conf. Exhib. Opt. Commun. (ECOC 2013)*, no. 1, pp. 1221–1223, 2013.

[45] N. K. Fontaine, “3D waveguide and all-fiber ‘photonic lantern’ spatial multiplexers,” *COIN 2014 - 12th Int. Conf. Opt. Internet*, pp. 3–4, 2014.

[46] R. Ryf, N. K. Fontaine, M. Montoliu, S. Randel, B. Ercan, H. Chen, S. Chandrasekhar, and A. H. Gnauck, “Photonic-Lantern-Based Mode Multiplexers for Few-Mode-Fiber Transmission,” no. Il, pp. 9–11, 2014.

[47] H. Bulow, H. Al-Hashimi, and B. Schmauss, “Coherent multimode-fiber MIMO transmission with spatial constellation modulation,” *2011 37th Eur. Conf. Exhib. Opt. Commun.*, pp. 1–3, 2011.

[48] N. K. Fontaine, R. Ryf, J. Bland-Hawthorn, and S. G. Leon-Saval, “Geometric requirements for photonic lanterns in space division multiplexing.,” *Opt. Express*, vol. 20, no. 24, pp. 27123–32, 2012.

[49] J. Bland-Hawthorn and P. Kern, “Molding the flow of light: Photonics in astronomy,” *Phys. Today*, vol. 65, no. 5, pp. 31–37, 2012.

[50] S. G. Leon-Saval, T. a Birks, J. Bland-Hawthorn, and M. Englund, “Multimode fiber devices with single-mode performance.,” *Opt. Lett.*, vol. 30, no. 19, pp. 2545–2547, 2005.

[51] J. Bland-Hawthorn and P. Kern, “Molding the flow of light: Photonics in astronomy,” *Phys. Today*, vol. 65, no. 5, pp. 31–37, 2012.

[52] S. G. Leon-Saval, T. A. Birks, J. Bland-Hawthorn, and M. Englund, “Multimode fiber devices with single-mode performance,” *Opt. Lett.*, vol. 30, no. 19, p. 2545, Oct. 2005.

[53] H.-J. Yu, Q. Yan, Z.-J. Huang, H. Tian, Y. Jiang, Y.-J. Liu, J.-Z. Zhang, and W.-M. Sun, “Photonic lantern with multimode fibers embedded,” *Res. Astron. Astrophys.*, vol. 14, no. 8, pp. 1046–1054, Aug. 2014.

[54] J. Bland-Hawthorn and P. Kern, “Astrophotonics: a new era for astronomical instruments,” *Opt. Express*, vol. 17, no. 3, p. 1880, Jan. 2009.

[55] B. Analui and A. Hajimiri, “Bandwidth enhancement for transimpedance amplifiers,” *IEEE J. Solid-State Circuits*, vol. 39, no. 8, pp. 1263–1270, 2004.

[56] J.-D. Jin and S. S. H. Hsu, “A 40-Gb/s Transimpedance Amplifier in 0.18- m CMOS Technology,” *IEEE J. Solid-State Circuits*, vol. 43, no. 6, pp. 1449–1457, 2008.

[57] P. Toliver, I. Ozdur, A. Agarwal, and T. K. Woodward, “Comparison of LIDAR system performance for alternative single-mode receiver architectures: modeling and experimental validation,” vol. 8731, no. 732, p. 87310W, 2013.

[58] F. Benzarti and H. Amiri, “Speckle Noise Reduction in Medical Ultrasound Images.,” *Adv. Break. Ultrasound Imaging*, no. June, p. 304, 2013.

[59] J. X. Chen and M. Li, “The Performance of Eye Diagrams and Bit Error Rates of Optical Fiber Communication System,” *Adv. Mater. Res.*, vol. 811, pp. 558–563, Sep. 2013.

[60] C. M. Grinstead and J. L. Snell, “Introduction to Probability,” *Swart. Coll.*, pp. 1–520, 2007.

[61] H. O. Lancaster, *The Chi-squared Distribution*. Wiley, 1969.

[62] the free encyclopedia From Wikipedia, “Chi-squared distribution.” [Online]. Available: https://en.wikipedia.org/wiki/Chi-squared_distribution. [Accessed: 15-Jun-2016].

[63] the free encyclopedia From Wikipedia, “Noncentral chi-squared distribution.” [Online]. Available: https://en.wikipedia.org/wiki/Noncentral_chi-squared_distribution. [Accessed: 15-Jun-2016].

[64] P. Gatt and S. W. Henderson, “Laser radar detection statistics: A comparison of coherent and direct detection receivers,” *Laser Radar Technol. Appl. Vi*, vol. 4377, pp. 251–262, 2001.

[65] G. P. (Govind P. . Agrawal, *Fiber-optic communication systems with cd*. Wiley, 2010.

[66] C. M. Sonnenschein and F. a Horrigan, “Signal-to-Noise Relationships for Coaxial Systems that Heterodyne Backscatter from the Atmosphere.,” *Appl. Opt.*, vol. 10, no. 7, pp. 1600–4, 1971.